

Review

Progress in module level quantitative electroluminescence imaging of crystalline silicon PV module: A review



Vishal E. Puranik, Ravi Kumar, Rajesh Gupta*

Department of Energy Science and Engineering, Indian Institute of Technology Bombay, India

ARTICLE INFO

Keywords:
 Quantitative electroluminescence imaging
 PV module
 Defect
 Degradation
 Characterization
 Solar cell

ABSTRACT

Electroluminescence (EL) imaging is a prominent tool for obtaining qualitative and quantitative information of defects and degradations in a crystalline silicon (c-Si) PV module. Quantitative EL imaging is an emerging field in which the impact of defects and degradation on module performance is evaluated from the EL images. However, the literature lacks an illuminated discussion on quantitative EL imaging compared to qualitative applications and implementation aspects of EL imaging. This article aims to provide one-stop information and a comprehensive review of advancements in module-level quantitative EL imaging. The state-of-art quantitative EL methods evaluating the module level impact of optical, bulk, series resistance, and shunting-related defects and degradations are reviewed. Each method has been critically assessed based on the approach of quantification, input EL imaging requirements, and performance of quantification. The outcome of the conducted assessment is concisely presented in the comparative table. It highlights the key achievements, advantages, and limitations of each method. Suggestions for future work are given to enhance quantification performance and overcome existing limitations for each method. Indoor and outdoor applicability for all the methods is briefly discussed, and on-field challenges are outlined considering the present use of outdoor EL imaging. Further, a comparative discussion of quantitative EL methods is presented for each category of defects and degradation to summarize the present stage of research, underlying research gaps, and future scope of work. This review paper would be instrumental for the future progress of quantitative EL imaging and its possible use in indoor or outdoor conditions.

1. Introduction

Crystalline silicon (c-Si) PV module is the prime source of solar power generation and shares 90% of the market [1,28]. Efficient and failure-free operation of c-Si PV module is crucial throughout its lifespan for the successful and profitable functioning of PV plant. Induction of various defects and degradation in a PV module is inevitable. Defects are normally get induced in the process of module manufacturing, shipping, and installations. In a field operation, environmental stressors such as high temperature and humidity cycles, hail-storming, snow-fall, high UV exposure, high voltage stress give rise to the induction of various defects and degradations in a PV module [1,50]. Defects and degradation affect short term (dropped module efficiency, mismatch-losses in a string) and long term (increased degradation rate) performance of a PV system [43,50,57,85]. Hence, timely diagnostics and performance evaluation of a defective PV module are essential for taking preventative measures to increase module lifetime and overall PV system performance.

Electroluminescence (EL) imaging is the most commonly used technique for spatial investigation of module defects and degradations [31–32,30,38]. In this paper, review of the quantitative use of EL imaging for assessing module level defects and degradations is presented.

1.1. Literature review

EL imaging was first introduced in 2005 for PV applications by Fuyuki et al. [32] for mapping minority charge carriers diffusion length in solar cells and identifying defective locations. It is based on the physical phenomenon of electroluminescence, in which material emits luminescence when excited electrically. Under the DC excitation, c-Si PV cell emits infrared (IR) radiation with wavelength of 1000–1300 nm, with a peak at 1150 nm, whose intensity depends on a cell biasing voltage [32]. EL imaging identifies localized cell defects as well as non-uniformity within a module [31,30]. IEC TS 60904–13 provides necessary recommendations for capturing EL images of a PV module and guidance for qualitatively identifying defects from the captured images.

* Corresponding author.

E-mail address: rajeshgupta@iitb.ac.in (R. Gupta).

Nomenclature	
EL	Electroluminescence
$I_{EL(i)}$	Local current
c-Si	Crystalline Silicon
I_{sc}	Short circuit current
PV	Photovoltaics
n	Carrier density
UV	Ultraviolet
L_e	Effective diffusion length
DC	Direct Current
ϕ_{EL}	EL intensity
IR	Infrared
$\phi_{EL(i,j)}$	Pixel EL intensity
$I-V$	Current-Voltage
$\phi_{EL(loss)}$	Average EL intensity reduction
LED	Light Emitting Diode
N	Total minority carriers/cells
EVA	Ethylene Vinyl Acetate
V_f	Forward bias voltage
CCD	Charge Coupled Device
V_t	Thermal voltage
InGaAs	Indium Gallium Arsenide
A	Voltage calibration constant
QE	Quantum Efficiency
A"	Current calibration constant
SDM	Single Diode Model
f-number	Aperture
DDM	Double Diode Model
I_{ph}	Light generated current
LID	Light-Induced Degradation
I_{01}, I_{02}	Saturation current
LeTID	Light and Elevated Temperature-Induced Degradation
n_1, n_2	Ideality factor
PERC	Passivated Emitter and Rear Contact
R_s	Series resistance
PID-s	Potential-Induced Degradation Shunting
$R_{s(i)}$	Local series resistance
ML	Machine Learning
	$R_{cell \text{ (average)}}$ Average series resistance per cell
	AI Artificial Intelligence
	R_{sh} Shunt resistance
	CNN Convolutional Neural Network
	R_{finger} Finger resistance
	ANN Artificial Neural Network
	R_{busbar} Busbar resistance
	k-NN k-Nearest Network
	R_{sheet} Lateral sheet resistance
	SVM Support Vector Machine
	V Voltage
	RF Random Forest
	$\Delta V_{Rs(i)}$ Local voltage drop across $R_s(i)$
	MPP Maximum Power Point
	V_{Rsh} Voltage across ohmic shunt
	STC Standard Test Conditions
	I_{Rsh} Current flowing through R_{sh}
	RMSE Root Mean Square Error
	V_{oc} Open circuit voltage
	QUELA Quantitative Electroluminescence Analysis
	R_{mod} Module series resistance
	ELMO Electroluminescence Power Prediction of Module
	V_{mod} Module voltage
	QUEL Quantitative Electroluminescence
	I_{mpp} Current at maximum power point
	DLIT Dark Lock-in Thermography
	V_{mpp} Voltage at maximum power point
	g-QUEL Generalized Quantitative Electroluminescence
	C_f Correlation constant/factor
	F _{BBCR} Busbar Corrosion Ratio Model
	P_{loss} Power loss
	$n_{p(x)}$ Injected carrier density
	$C_{\phi_{EL}}$ PID-s index
	$n_{p(0)}$ Injected carries at the junction
	V_{op}^n Cell voltages
	P_{out} Output power
	x Distance from junction
	I_{EL} EL current
	L_e Effective diffusion length

Initially, EL imaging was limited to laboratory research, a fast inspection of cell defects in a production line, and module quality check. In the last decade, outdoor EL inspection has become popular mainly due to advancements in EL imaging systems and aerial drone technology for identifying defects and degradations in a field operational PV module [24,42,78]. Recently published review papers have thoroughly discussed the trends in outdoor PV inspection and implementation aspects of EL imaging [37,41,50,54], which are presented in Table 1.

The reported review papers (Table 1) have mainly discussed outdoor implementation aspects of EL imaging. Based on the captured EL images existing defects and degradation in a module can be qualitatively investigated by conventional approaches or machine learning methods refer!! [7,27,38,45,67,82]. Qualitative assessment of a PV module does not provide information related impact of defects on module parameters and performance. For predicting future performance, optimize a plant operation, or take preventive measures against degradation, quantitative performance evaluation of a PV module is essential. Current-voltage ($I-V$) measurement is the standard tool to measure output power (P_{out}) of a PV module. However, it does not reveal the possible reasons for module under-performance and spatial information of existing defects and degradations. Also, on-field use of $I-V$ technique is quite cumbersome, involves the intervention of plant operation, and can be tedious for large number of modules in a big PV field. EL imaging provides cell

Table 1

Brief summary of recently published review articles in the field of EL imaging.

Publication	Work contribution
[41]	<ul style="list-style-type: none"> This paper has reported an outdoor EL method to monitor the performance of a PV module The proposed differential EL method can capture EL image in a day time Also, discussed the estimation of cell voltage from EL images for the quantitative analysis of a PV module
[37]	<ul style="list-style-type: none"> This paper has presented review of different IR and luminescence imaging techniques used for monitoring large scale power plants. The use of EL imaging has been discussed considering the outdoor challenges, complexity of image acquisition, and compatibility with unmanned aerial inspection
[50]	<ul style="list-style-type: none"> This paper has presented review of module degradations, their economic impact, and field inspection techniques, including EL imaging. Matrix of module degradation and corresponding suitable inspection techniques used have been discussed
[54]	<ul style="list-style-type: none"> This paper has been dedicated to luminescence imaging and thoroughly discussed the outdoor implementation aspects of EL imaging. Different technical aspects involved in day or night time EL imaging, including imaging set-up (ground or aerial), camera technology, and software requirements, have been well discussed.

level spatial information of a PV module and is capable of inspecting large PV field at night hours, which becomes a strong motivation for quantitative EL imaging to evaluate module performance from the EL images.

1.2. Quantitative EL imaging

Quantitative EL imaging was initially used to estimate sub-cell and cell level parameters of a c-Si PV cell [11,33,35,84]. In 2010, it was first taken to a module level by Potthoff et al. [66] for estimating operating voltages and series resistance of an individual cell within a module. Fig. 1 shows the number of publications reported in recent years in the field of qualitative and quantitative application of EL imaging for assessing PV module. It may be observed that quantitative EL imaging is an emerging field compared to qualitative EL imaging. Increased number of papers on qualitative EL imaging is mainly due to the increasing use of machine-learning (ML) based techniques for automatic classification and identification of defects and degradations.

In the past seven years, researchers have reported quantitative EL methods based on different approaches to assess the impact of various defects and degradation. For evaluating the impact cell breakages, Castañeda et al. [13] and Hoffmann et al. Rodrigues et al. [36,74] have reported analytical and machine learning methods, respectively, in which power loss caused by cell breakages has been estimated. Soiling is one of the frequently observed problem in which the accumulation of dust particles results on module surface. Doll et al. [23] have proposed an empirical method to estimate soiling power loss from EL images. Fruehauf et al. [29] and Rajput et al. [71] have proposed novel approach to extract individual cell bulk diode parameters and series resistance from the EL images for simulating module performance. Karimi et al. [46] used machine learning approach to quantify module series resistance, which increased due to corrosion. Potential-induced degradation shunting (PID-s) is one of the severe degradation modes that causes significant power loss. Bedrich et al. [6], have proposed an empirical method to estimate PID-s loss from two EL images. Kropp et al. [51] and Puranik and Gupta [69] have reported parametric extraction-based approaches to simulate the performance of a PID-s affected module from EL images. Few papers [15,70] have considered multiple defects and degradation in the quantification of c-Si PV module. The combined use

the
other
way

of EL imaging with I-V measurements [22] or dark lock-in thermography (DLIT) [3] has also been reported for quantitative analysis of PV module.

In the literature, implementation aspects of EL imaging (Table 1) have been well reviewed and discussed. Also, Fig. 1 shows that significant emphasis has been given to the qualitative use of EL imaging for investigating defective modules. In that comparison, quantitative EL imaging is an emerging field and less discussed in the literature. While considering its potential, a thorough analysis of existing literature is essential for its future growth. From that perspective, this paper aims to provide a critical technical review and one-stop information on the progress of module level quantitative EL imaging for evaluating the impact of various defects and degradations. Based on the type of defect and degradation, the quantitative EL methods have been categorized into four classes optical defects, bulk and series resistance issues, shunting, and multi-defects and degradation. The detailed assessment of each literature method is conducted based on the performance of quantification (accuracy of prediction; level of quantification (cell/module level)), input EL imaging requirements (number of EL images, image processing requirements, auxiliary measurements or datasheet information), and approach of quantification (parametric/empirical/machine learning/multi-characterization). The outcome of the assessment for each method has been presented in tabular form comparative analysis. The key achievements, merits, indoor or outdoor applicability, and limitation of each method have been presented. Recommendation for future work has been given for each method to improve the performance of quantification, overcome the existing limitation, and increase the applicability. Further, the reported EL methods are comparatively discussed for each category of defects and degradations to highlight the present stage of research, underlying research gaps, and possible future scope of work.

The organization of this review article is depicted in Fig. 2. Section 2 provides the necessary background knowledge for understanding the quantitative EL method and analysis presented in subsequent sections. In this Section, the introduction of EL imaging, covering theory and working principle, a brief description of image acquisition and correction procedures is presented. Further, an overview of qualitative applications of EL imaging for investigating different types of defects and degradation in a c-Si PV module are presented. Section 3 presents a detailed literature review of module-level quantitative EL imaging. It starts with a brief discussion of cell-level quantitative EL imaging. Further, it presents the state-of-art module level quantitative EL methods reported for various defects and degradation. In Section 4 detailed summary of the literature and outcome of the conducted assessment for each method is presented in comparative table. In Section 5, discussion and future scope of work in module level quantitative EL imaging for different classes of defects and degradation is presented. Section 6 concludes this article by summarizing key findings, identified research gaps, and future scope of work in point-wise manner.

2. EL imaging: Fundamentals and application to PV module

This section presents the fundamentals of EL imaging and its applications to PV cells and modules. The first part presents the theory and working principle of EL imaging, including optical and material properties of a c-Si cell, a description of EL setup components, different PV cell models, and EL characteristics. In the second part, EL imaging acquisition and image correction procedures have been presented. The third part presents different approaches for qualitatively detecting defects and degradation from EL images.

2.1. Theory and working principle

Fig. 3(a) shows the block diagram of an EL inspection system generally used for indoor applications. Indoor EL imaging is performed in dark conditions. Specimen PV cell or module is excited using programmable power supply, which works in synchronization with EL

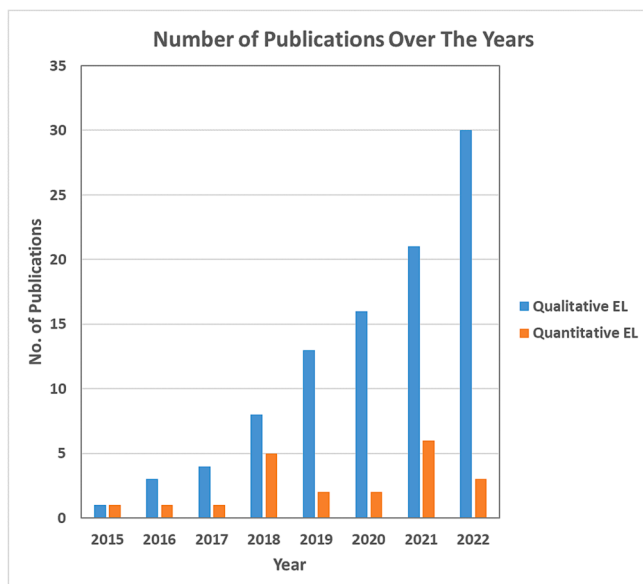


Fig. 1. Number of publications over the years on qualitative and quantitative EL imaging (obtained from the Scopus yearwise search with the following keywords: Electroluminescence Imaging; Photovoltaic; Defect Detection; Performance; Quantitative; Parameters).

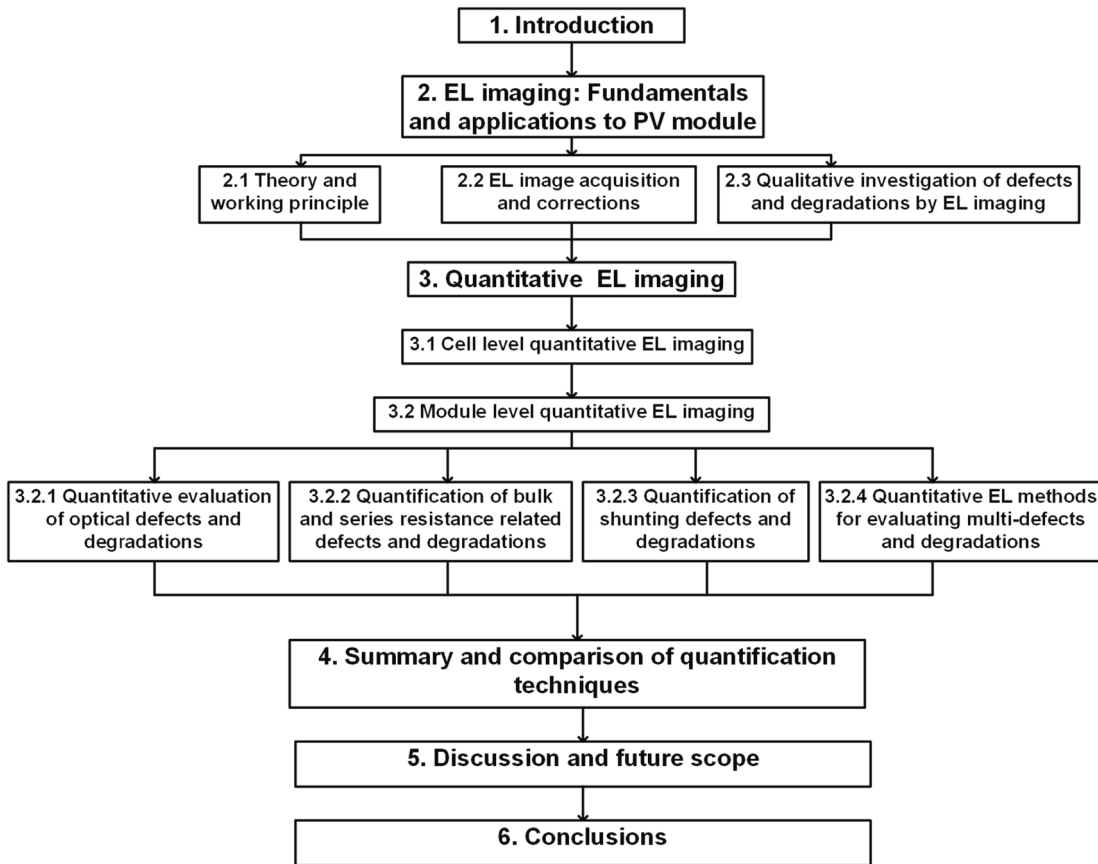


Fig. 2. Block diagram showing content analysis of the paper.

camera and is controlled through EL software. Typical magnitude of applied EL current (I_{EL}) \leq rated short circuit current (I_{sc}) of a test module. Fig. 3(b) shows the mechanism of EL emission; biasing leads to injection of minority carriers at the $p-n$ junction depending on the applied voltage. Injected excess minority carriers fall exponentially with distance as per Eq. (1) [32,30].

$$n_{p(x)} = n_{p(0)} \exp(-x/L_e) \quad (1)$$

$n_{p(x)}$ -injected carrier density, $n_{p(0)}$ - injected carries at the junction, x -distance from junction, L_e -effective diffusion length.

Radiative recombination resulting between the minority and majority charge carriers leads to emission of an EL signal. Intensity of EL emission (ϕ_{EL}) is proportional to the total number of injected minority carriers (N) which depends on forward voltage (V_f). Fig. 3(c) shows a simplified equivalent circuit of a PV cell under dark EL conditions. In a healthy cell, applied EL current flows through a bulk $p-n$ junction diode; hence, relation between V_f and I_{EL} can be expressed as,

$$I_{EL} = I_{01} \exp\left(\frac{V_f}{n_1 V_i}\right) \quad (2)$$

I_{01} and n_1 are reverse saturation current and ideality factor of bulk $p-n$ junction diode, respectively. Fuyuki et al. [31–32,30] have experimentally studied the relationship between V_f , I_{EL} , and ϕ_{EL} . It has been shown that a cell ϕ_{EL} follows an exponential relation with V_f as Eq. (3),

$$\phi_{EL} = A \exp\left(\frac{V_f}{V_i}\right) \quad (3)$$

A is voltage calibration constant, cumulatively representing the effect of module external quantum efficiency, black body radiations, and EL system parameters [73]. From Eq. (2) and (3), the relation between cell ϕ_{EL} and I_{EL} can be derived as [31],

$$\log(\phi_{EL}) = A'' + n_1 \log(I_{EL}) \quad (4)$$

A'' is current calibration constant of an EL system, and it can be expressed as the function of voltage calibration constant and $p-n$ junction diode parameters as Eq. (5) (derived from Eq. (2) and (3)) [69]

$$A'' = \log(A) - n_1 \log(I_{01}) \quad (5)$$

Fig. 3(d) shows the spectrum of Si EL emission [32], which lies in IR region with peak around 1150 nm and distributed between 1000 and 1300 nm due to the indirect band gap nature of Si. In EL conditions, PV cell can be seen as poor light emitting diode (LED) with no visible light. Glass, and EVA are nearly transparent to emitted EL signal. EL camera captures IR light, which is placed with optical axis perpendicular to cell for better collection of EL signal. EL camera consists of optical lens which is transparent to desired IR range. As per requirement, lens can be of wide to narrow angle focal length. Lens aperture (f -number) allows controlling the EL intensity, depth of field, and sharpness of EL images. Camera is generally focused by manually adjusting working distance between EL camera and test module. Long pass filter is placed before the detector with cut-off frequency 850 nm, which ensures the attenuation of any visible light presence in surrounding. For high quality images dark environment is preferred to reduce the effect of stray light, even though EL images can be captured in the presence of mono-chromatic light with wavelength $<$ filter cut-off frequency.

Camera detector converts IR light into an equivalent electrical signal to produce an EL image of a test cell or module. Fig. 3(e) shows the external quantum efficiency (QE) of Si-CCD and InGaAs detectors normally used in EL imaging [4]. Si-CCD sensors are a popular choice for indoor use due to their low cost and high spatial resolution (>10 M) [54]. Although QE is poor in Si spectrum range, providing few seconds (1–20 sec) long exposure, Si-CCD camera provides EL image with device's ability to convert light into electrical current

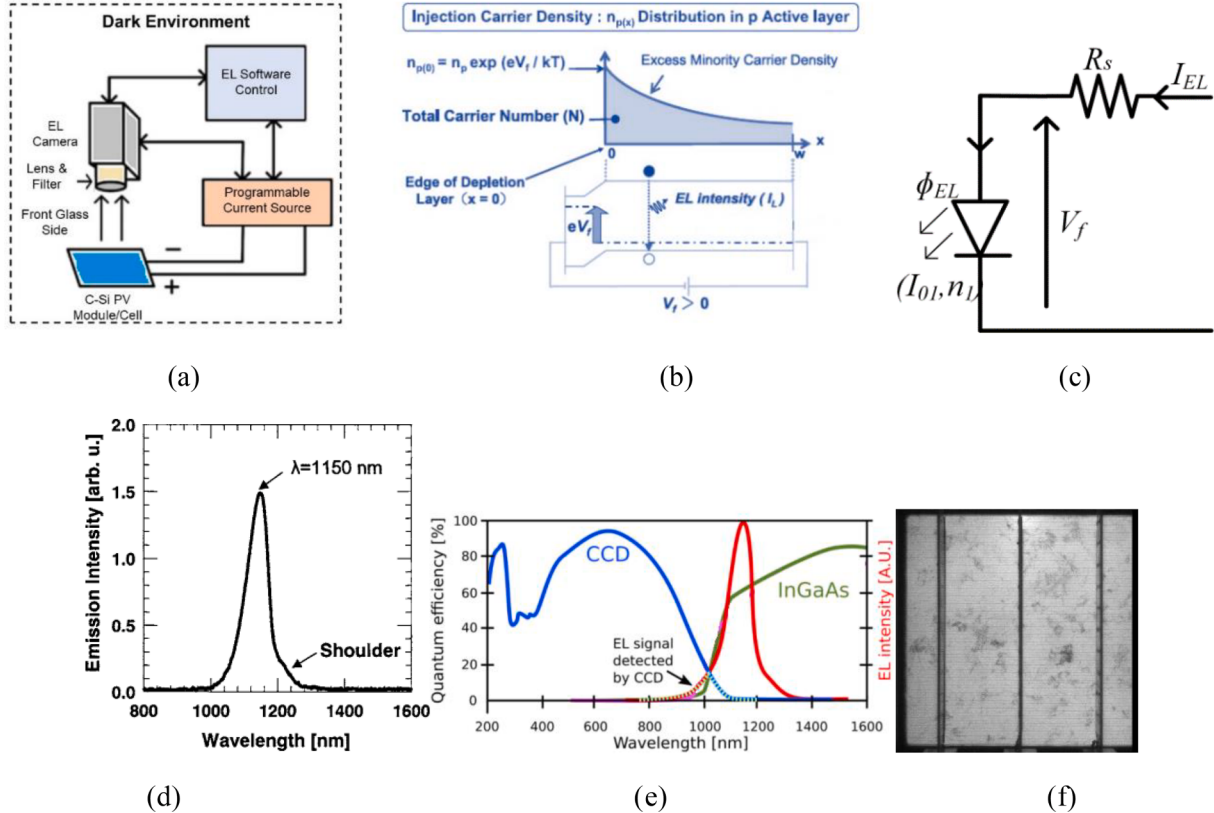


Fig. 3. (a) Block diagram of indoor EL set up (b) Mechanism of EL emission (reproduced from [30]) (c) Simplified equivalent circuit of a healthy PV cell under dark EL conditions (reproduced from [69]) (d) Si emission spectrum (reproduced from [32] with permission) (e) Si emission spectrum and sensitivity of Si-CCD and InGaAs sensors (reproduced from [4]) (f) EL image of multi c-Si cell.

sufficient brightness required for analysis. **InGaAs** sensor has higher QE in the range of Si spectrum. Hence, it can capture EL images in order of few ms (0.2–50 ms), making it most suitable for outdoor applications [54]. However, on the limitation side, it is very expensive and has limited spatial resolution (~1.3 M). Fig. 3(f) shows the captured EL image of multi c-Si PV cell. The dark spot in the EL image shows the sites within a cell with non-radiative recombination.

For quantitative performance evaluation of a PV cell, **single diode model (SDM)** and **double diode model (DDM)** are used, as shown in Fig. 4(a) and (b), respectively. SDM is more often used in the literature as it is simple to implement, although inaccurate at low irradiance levels. For higher accuracy and modeling of shunting defects and degradations, DDM is preferred [64]. Fig. 4(c) shows the **PV cell equivalent circuit under dark conditions** used for quantitative performance analysis. For spatial or sub-cell level quantitative analysis **distributed diode model** is used (Fig. 4(d)) [59] in which local potential at any particular point (i, j) within a cell can be estimated using Eq. (6).

$$V_{f(i,j)} = V_i \log\left(\frac{\phi_{EL(i,j)}}{A_{(i,j)}}\right) \quad \text{how to find } A_{(i,j)} ?? \quad (6)$$

Fig. 5 (a) and (b) shows the $I_{EL}-\phi_{EL}$ and $V-\phi_{EL}$ characteristics of a healthy PV cell, respectively. Defect free cell has almost linear $I_{EL}-\phi_{EL}$ curves on log-log plot [31], which is also expected from Eq. (4). Cell ideality factor determines a slope of $I_{EL}-\phi_{EL}$ characteristic for mono c-Si cell has n_1 [1–1.05] whereas multi c-Si cell has n_1 [1.1–1.2] [31]. Fig. 5 (b) shows the difference between $V-\phi_{EL}$ and $V_f-\phi_{EL}$ characteristics of a PV cell. From Eq. (3), $V_f-\phi_{EL}$ curve of a PV cell is expected to be linear on semi-log plot [66]. Referring to Fig. 4(c), for low EL current, $V = V_f$ due to negligible drop across R_s of a cell; hence, both curve coincides. For high EL current, $V-\phi_{EL}$ curve becomes non-linear due to the increased voltage drop across cell R_s . Therefore, to determine cell or module calibration constant (A) from Eq. (3), low EL current ($\leq 0.1I_{sc}$) is used [66]. Fig. 5 (c) shows the $V-I_{EL}$ and $V-\phi_{EL}$ characteristics of a PV cell. It may be observed that a cell emits EL emission for $V > 0.4$ –0.45 V, which

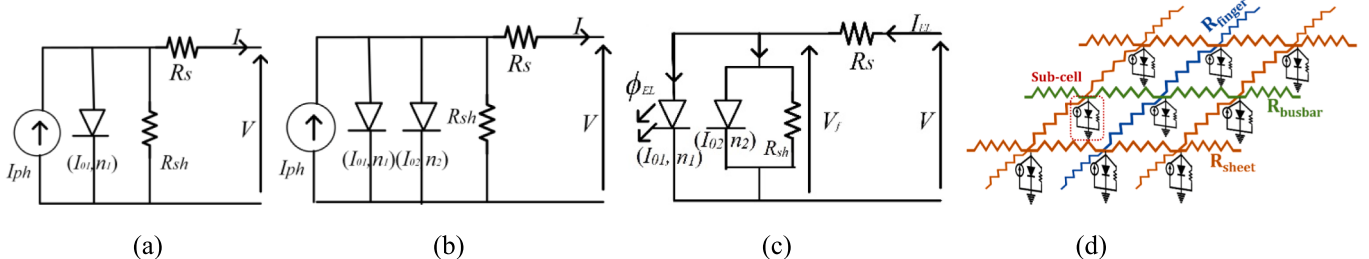


Fig. 4. (a) SDM model [60] (b) DDM model [40] (c) Equivalent circuit of a cell in dark conditions [70] (d) Distributed diode model of a cell (reproduced from [59]). I_{ph} - light generated current, I_{01}, I_{02} - reverse saturation currents of bulk and recombinative diode, n_1, n_2 - ideality factors of bulk and recombinative diode, R_s, R_{sh} - parasitic series and shunt resistances, R_{finger} - finger resistance, R_{busbar} - busbar resistance, R_{sheet} - lateral sheet resistance.

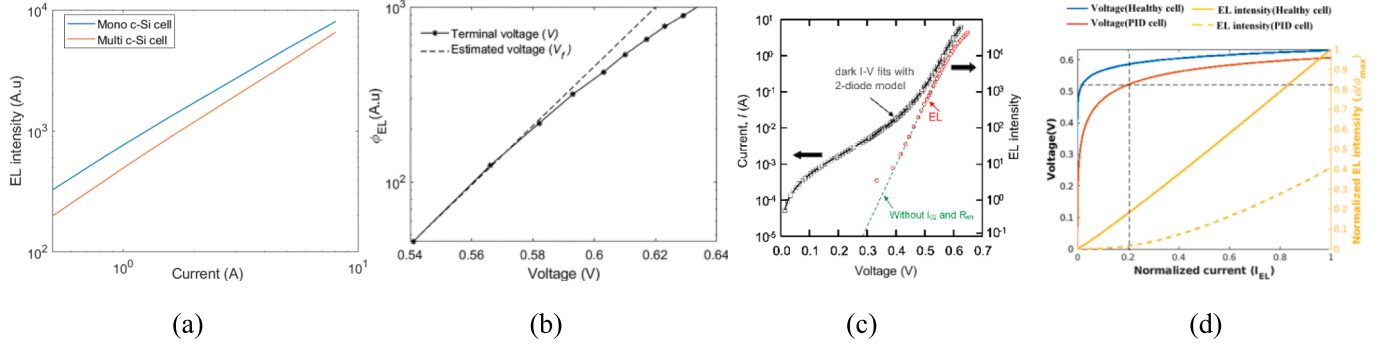


Fig. 5. (a) Cell I_{EL} - ϕ_{EL} characteristic (b) cell V - ϕ_{EL} characteristic (reproduced from [70] with permission) (c) I - V and V - ϕ_{EL} characteristic of a PV cell (reproduced from [30]) (d) I_{EL} - V and I_{EL} - ϕ_{EL} characteristic of the healthy and shunted (PID-s affected) cell (reproduced from [68] with permission).

is the typical turn-ON voltage of a c-Si PV cell, it depends on the semiconductor properties of a bulk $p-n$ junction diode, and cell temperature [30]. Fig. 5(c) implies that the **current that flows through a bulk diode (Fig. 4 (c)) is only responsible for EL emission**. Current sink by recombinative diode and R_{sh} (see Fig. 4 (b)), does not contribute to ϕ_{EL} [68]. Fig. 5(d) compares healthy and shunted cell characteristics. It may be observed that the shunted cell emits EL signal at an excitation current corresponding to turning ON of bulk diode, e.g., $0.2I_{sc}$ for the test cell. As the severity of shunting increases, magnitude of I_{EL} at which cell emission results also increases [68].

2.2. EL image acquisition and image corrections

Indoor acquisition of EL images is normally conducted in the dark conditions (Fig. 3(a)). For better collection of an EL signal, a test PV module is place normal to the optical axis of the EL camera, and excited by a current source normally keeping $I_{EL} \leq I_{sc}$. Generally, for looking for

R_s -related defects EL images are captured at I_{sc} and for R_{sh} related $0.1I_{sc}$ is used (Technical Specification IEC TS 60904-13, 2018) [38]. However, EL images can be captured at number of required currents as per requirements. Outdoor EL inspection is performed in a day as well as night conditions. Recent review papers (see Table 1) have presented detailed technical aspects of outdoor EL imaging. In night, it is possible to use low-cost Si-CCD camera that enables capturing high-definition EL images even of strings containing multiple modules simultaneously. InGaAs camera is preferred in day time EL imaging due to its high capturing speed [54]. EL camera is mounted either on ground-based stationary set up such as a tripod, or multi-bridge system [54]. Stationary ground-based system using tripod/multi-bridge allows capturing high-resolution EL images of modules for detailed performance analysis. Whereas for scanning large volume of PV system in short time or installations which are difficult to access, such as facade, roof tops, drone-based aerial inspection is a good choice [37,54].

Captured EL images require corrections prior to processing

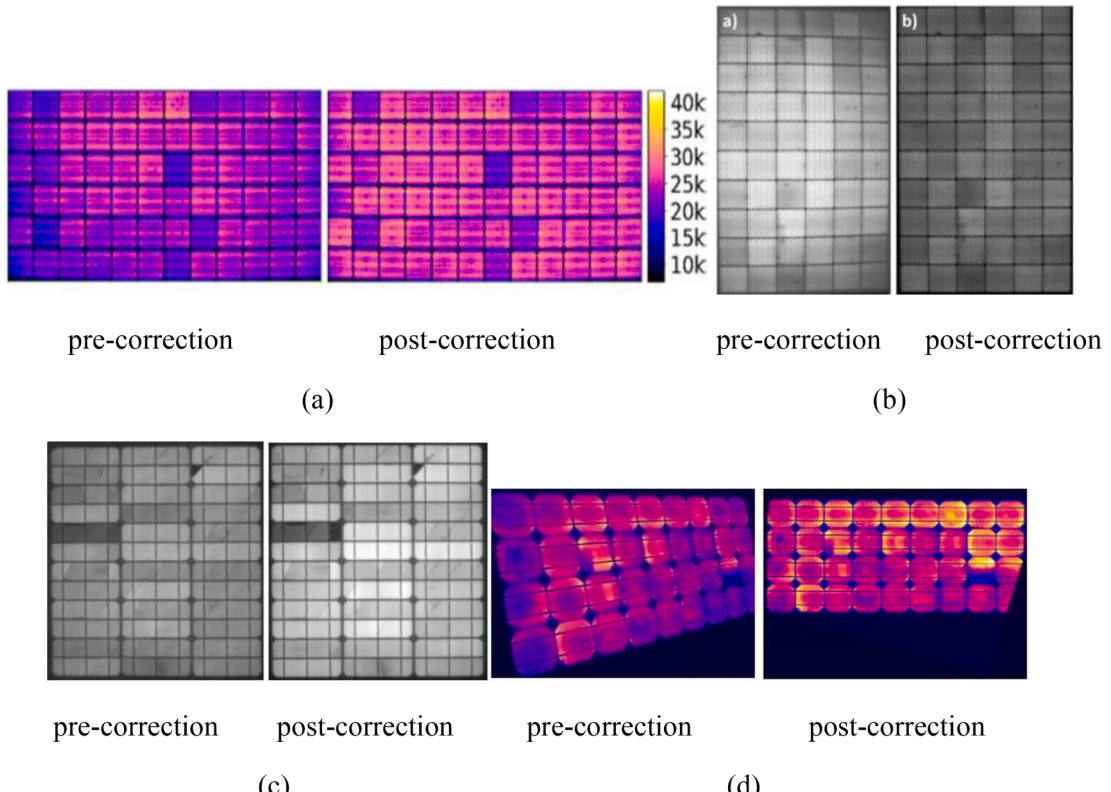


Fig. 6. (a) Vignetting corrections (reproduced from [5]) (b) lens distortion correction (reproduced from [18]) (c) Background noise elimination (d) Correction for perspective distortion (reproduced from [4]).

quantitative evaluation. Requirement of image correction depends on the scope of work. For simple visual inspection, most image corrections may not be required apart from scaled EL image with good Signal-to-Noise Ratio (SNR). However, for quantitative evaluation it is essential to apply necessary image correction to eliminate the effect of artefacts. Some of the essential image corrections performed prior to processing of EL images are described below.

2.2.1. Vignetting correction

Vignetting is known for reduction in cell EL intensity or image brightness at the periphery compared to centre of image (Fig. 6(a)). Normally it is observed when using wide angle lens with lower focal length and setting small f -number (greater aperture). Vignetting can be minimized by positioning module at the centre of field of view, using high f -number and lens with higher focal length. Otherwise, vignetting correction procedure need to be followed as described in (Technical Specification IEC TS 60904–13, 2018) [38].

2.2.2. Barrel distortion

Curvilinear shape of lens causes fishy eye view of captured EL image as shown in Fig. 6(b). Lens distortion mainly result in case of wide-angle lens with lower focal length. Barrel distortion can be minimized either using narrow-angle lens with larger focal length or following image correction procedure for barrel distortion given in [4].

2.2.3. Background frame subtraction and bad pixel removal

In order to remove the effect of sensor noise, stray light, or reflected EL signal, unbiased EL image of a PV module is subtracted from biased EL image. Also, any failed pixel needs to be corrected for proper scaling of images which is required for visual inspection. Fig. 6(c) highlights the difference between EL image without correction and with correction.

2.2.4. Perspective correction

Module appears trapezoidal shape rather than rectangular in an EL image due to non-perpendicular angle between EL camera and module. Bedrich [4] have presented a detailed procedure for perspective corrections; Fig. 6(d) show an EL image of a module pre and post-correction.

2.3. Qualitative investigation of defects and degradations by EL imaging

This section briefly introduces different categories of defects and degradation in a c-Si PV module, followed by the methods used to investigate defects and degradations from the EL images.

2.3.1. Defects and degradations in c-Si PV module

Defects and degradations in a c-Si PV module can be classified based on the affected cell parameters. Optical defects and degradations reduce the photo current generation either by reducing amount of light reaching to a cell or decreasing active cell area. It reduces cell I_{ph} , thereby reducing module I_{sc} . Discoloration, delamination, soiling, and cell breakages are some major I_{ph} -related issues [1,50]. Discoloration progresses at the centre of a cell in which encapsulant colour changes from light yellow to dark brown due to UV exposure resulting 6–13% reduction in short circuit current [49,79]. In delamination, loss of adhesion occurs at the interface of cell-encapsulant or cell-backsheet. Due to increased reflections may result up to 4% of performance loss [1,49]. Accumulation of dust, air pollution, growth of microbial algae, or bird droppings on the module surface leads to soiling [1]. Soiling causes uneven shading of PV module, which may result 10–30% of power loss. Cell breakage electrically disconnects a part of cell (type-C crack) and decreases cell area [1,50].

Bulk degradation causes changes in the cell bulk semiconductor properties affecting the I_{01} and n_1 parameters of a cell. It includes light-induced degradation (LID), light and elevated temperature-induced degradation (LeTID), manufacturing mismatches, and non-uniform

aging of cells. LID is known for decreasing module efficiency after the installation due to first exposure to light. In LID, oxygen atoms form a defect with boron via carrier-induced recombination mechanism under sunlight [55,80]. In amorphous silicon PV modules, the performance loss is found in the order of 15%, while in c-Si modules, loss is between 3 and 6% [1,50]. LeTID is mainly observed in p-type passivated emitter rear contact (PERC) cells. Compared to LID, it occurs at high temperature above 50 °C. Although LeTID mechanism is not fully understood yet, hydrogen concentration is considered one of the causes [14]. LeTID progresses non-uniformly in a PV module and may cause 10–16% of power loss [19,47].

Series resistance-related problems mainly include cracks (Mode A and B), finger breakages [52], busbar interconnect failure [16], and corrosion [79]. Crack in c-Si cells occur due to mechanical and thermal stresses experienced by a module. Cracks are generally classified into three categories Mode A, B, and C depending on their severity [38,81]. Mode A crack has small width, and it can be seen as a line defect in EL image without causing any power loss. Mode B cracks generally have large widths that exhibit an increase in the resistance thus, increased contrast between active and defective regions can be observed in high current EL image. Mode C cracks cause a complete electrical separation of a defective area from a cell which appears completely dark in EL images. Impact of a crack can vary from insignificant to complete failure depending on its size and orientation [1,50]. Finger breakages and busbar interconnect failure are mainly induced by thermo-mechanical fatigue and bad soldering, resulting in high series resistance. The deterioration of any PV module component can increase the water and oxygen penetration which can facilitate corrosion [1,49,50].

PID-s, recombinative site, process-induced shunt, and deep backsheet scratches are some major shunting defects. Shunt-related defects and degradation changes recombinative diode parameters (I_{02} , n_2) and R_{sh} of a cell. If change in recombinative diode parameters (I_{02} , n_2) is more than R_{sh} , shunting is known as non-ohmic; otherwise, if change in R_{sh} dominates, then shunting is known as ohmic shunting [67]. Also, based on the severity level, shunts can be called as weak or strong shunts [11]. Weak shunting defects cause low power loss and do not lead to complete cell darkening in low current EL images ($0.1I_{sc}$ or $0.2I_{sc}$). Strong shunting defects cause considerable power loss, leading to cell darkening at low current EL image. PID-s is mainly caused by the potential difference between the module frame and solar cells in a PV system. Depending on severity, PID-s may cause up to 30% of performance loss [56,65]. Recombination defects in a PV cell result in loss of charge carriers, which reduces the performance loss of a PV cell [12]. Process-induced shunts can result during fabrication, whereas deep backsheet scratches may result during transportation and installation [75].

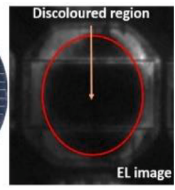
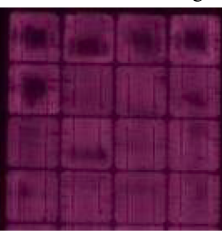
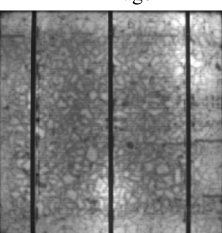
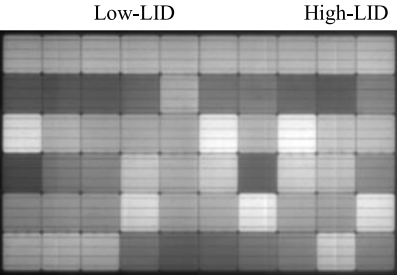
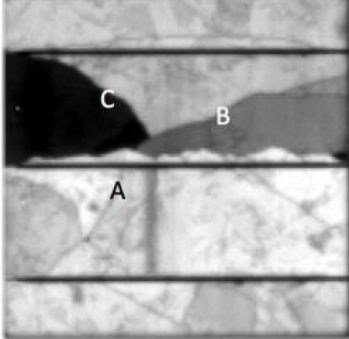
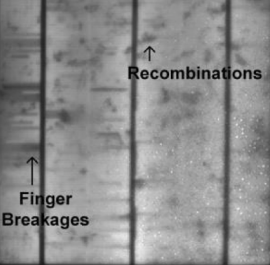
2.3.2. Detection using visual inspection of EL images

Visual inspection of EL images is the conventional way of identifying defects and degradations in a PV module. Spots showing less intensity or dark appearance in an EL image are considered defective areas within a cell. Defects and degradations in a c-Si PV module can be investigated from EL images based on their specific pattern or image features. Table 2 shows the detectable image features of some predominantly observed defects and degradations.

In high current EL images (captured at I_{sc}), non-uniformity within a cell caused by cracks, finger breakages, busbar interconnect failure, which increases local R_s is easily detected. Whereas low current EL images (captured at 0.1 or 0.2 I_{sc}) enable the identification of shunt-related defects as cell show dark appearance as compared with healthy cells.. For reliable detection, the use of two EL images ($0.1I_{sc}$ and I_{sc}) is recommended in the literature [38,68]. Optical defects and degradation, such as discoloration, delamination, or soiling, attenuate EL signal emitted by a cell. However, optical defects do not show consistent patterns in EL images. Initial to moderate phase of discoloration, localized spots of delamination or soiling are difficult to

Table 2

Distinguishable EL image features of different defects and degradations.

Defect/Degradation	Visibility in EL Image	Feature Description
Discoloration [53]	 	<ul style="list-style-type: none"> • Discolored region attenuates EL signal; hence defective region shows dark appearance in EL images • The blockage in EL is seen mostly at the center of cell in both low and high EL current images
Delamination [77]	 	<ul style="list-style-type: none"> • Delamination creates gap between the cell and glass, which reduces the EL intensity of defective region • Blockage due to delamination does not show clear correlation between dark portion in EL images and delamination
LID [26]	 	<ul style="list-style-type: none"> • LID results in increase in bulk recombinations due to presence of Boron-oxygen defects • LID results in drop in EL intensity of a cell
LeTID [50]		<ul style="list-style-type: none"> • Module affected by LeTID show non-uniform EL intensity in EL image, where defective cell show decreased intensity compared to healthy cells • Darkness is seen more in low EL current image as compared to high EL current image
Cracks (Mode-A, Mode-B and Mode-C) [38]		<ul style="list-style-type: none"> • Mode A can be seen as a line defect • Mode B cracks exhibit an increase in the resistance, which show uniform reduction in EL intensity • Mode C cracks electrically disconnect the defective area, which appears completely dark in EL images
Finger Breakages [68]		<ul style="list-style-type: none"> • Finger breakages increases the resistance for current hence resulting in drop in EL intensity • In high EL current image, uniform line defects with decreased intensity is visible at the location of finger breakages

(continued on next page)

Table 2 (continued)

Defect/Degradation	Visibility in EL Image	Feature Description
Busbar Interconnect Failure [16]		<ul style="list-style-type: none"> Busbar interconnects failure causes non-uniform distribution of current within a cell. Area nearby to active busbar shows the brightest appearance, and EL intensity decreases with distance due to non-uniform current distribution
PID shunting [50]		<ul style="list-style-type: none"> PID-s generally progress in the corner cells of a field-operational module. Corner cells show dark appearance in the EL images.
Process-induced shunts [68]		<ul style="list-style-type: none"> Process-induced shunts cause a drop in cell intensity depending on its severity Shunted cell appears dark in low current EL image

differentiate from other defects using EL images. Hence sole EL imaging may not be reliable for confirming the optical defect type therefore require manual inspection along with EL imaging. Visual inspection of EL images is simple way; however, for inspecting large PV field it is not possible to inspect an individual PV module. Hence, in recent years, deep machine learning (ML) based approaches (Section 2.3.3) have been reported for the automatic identification of defects and degradations.

2.3.3. Detection using machine learning

For inspecting large PV fields using EL imaging, different artificial intelligence (AI)/ML-based deep learning algorithms such as convolutional neural networks (CNN), artificial neural network (ANN), k-nearest network (k-NN), support vector machine (SVM) and random forest (RF) have been proposed, in the recent years (Table 3). These algorithms are machine learning classifiers that categorize the cells based on different EL features. ML algorithms are firstly trained using a large set of EL images of different module types with manually pre-identified or marked defects and degradations. These trained algorithms automatically identify defects and degradations in the EL images (see Fig. 7), almost independent of cell size and module. The strengths, weaknesses, and potential applications of some important ML algorithms are presented in Table 3 that are used for qualitative assessment of PV modules.

3. Quantitative EL imaging

This section presented the review of the quantitative application of EL imaging for evaluating PV module performance. Section 3.1 presents brief review of cell level quantitative EL imaging. In Section 3.2, a detailed review of the quantitative EL method evaluating module level impact of various defects and degradations have been presented.

3.1. Cell level quantitative EL imaging

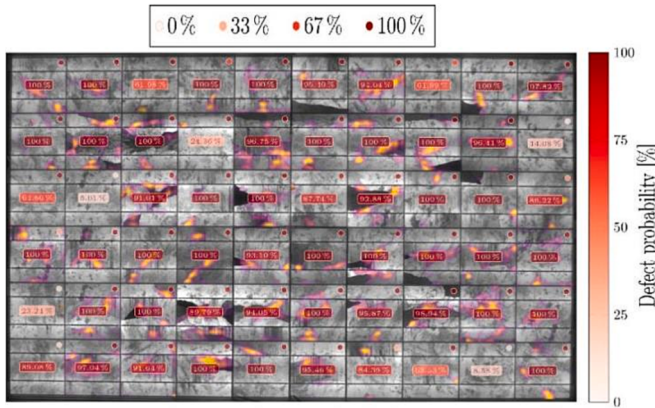
Cell level quantitative EL imaging is performed to find the impact of defects on cell output. In the literature, cell level quantitative EL imaging has been of two types, one is evaluating **spatially resolved parameters** [11,25,35,48] and second is based on **estimation of lumped parameters of a cell** [61,66].

Fuyuki et al. [32] has reported the semiquantitative relationship for mapping the minority carrier diffusion length based on spatial variation of EL intensity over a cell area. Hinken et al. [35] and Trupke et al. [84] have demonstrated the estimation of R_s and its lateral variation in mono c-Si cell. Whereas, Ory et al. [62] have estimated the spatially resolved R_s image of a multi c-Si PV cell (Fig. 8(a)), showing defective locations with increasing value of R_s . In the estimation of spatially resolved cell parameters, mainly analytical equations are derived from fundamental EL expressions like Eq. (6), in which the parameter of interest is expressed as the function of pixel EL intensity $\phi_{EL(i,j)}$, which varies over

Table 3

Comparison of different machine learning algorithms.

ML Algorithms	Strengths	Weaknesses	Potential Application
Convolutional Neural Networks (CNN) [2,20,21,45,46]	<ul style="list-style-type: none"> Excellent for image classification and feature extraction Captures spatial relationships in images Handles complex patterns and hierarchical features 	<ul style="list-style-type: none"> Requires large amounts of labelled data Computationally intensive Prone to overfitting with limited data 	<ul style="list-style-type: none"> Detection of defects and degradation in a PV module from images Identifying specific types of defects based on image analysis
Artificial Neural Network (ANN) [76]	<ul style="list-style-type: none"> Versatile and can handle various types of data Can capture complex relationships between features Handles nonlinear relationships Simple and easy to understand No training phase, as it memorizes the training data Can handle both classification and regression tasks 	<ul style="list-style-type: none"> Requires careful tuning of hyperparameters Prone to overfitting with limited data Black box model, lacks interpretability Computationally expensive during prediction Sensitive to irrelevant and noisy features Requires careful selection of the optimal k value 	<ul style="list-style-type: none"> Detection of defects and degradation based on input features Predicting the severity of defects or degradation
k-Nearest Network (k-NN) [7,21,63,76]			<ul style="list-style-type: none"> Classification of defects in electroluminescence images Anomaly detection by identifying patterns different from normal PV modules
Support Vector Machine (SVM) [20,21,45,58,63,76]	<ul style="list-style-type: none"> Effective in high-dimensional spaces Robust against overfitting Can handle both linear and nonlinear relationships with kernel trick 	<ul style="list-style-type: none"> Requires appropriate kernel selection and tuning Can be slow on large datasets during training Limited interpretability with complex kernels Lacks interpretability compared to individual decision trees It can be slow during prediction for large forests It may not work well with noisy data 	<ul style="list-style-type: none"> Classification of defects and degradation levels Boundary detection to identify regions of potential issues
Random Forest (RF) [21,45,58,63]	<ul style="list-style-type: none"> Robust against overfitting Handles high-dimensional data well Provides feature importance ranking Efficiently handles large datasets 	<ul style="list-style-type: none"> Identification of important features for defect and degradation detection Classification and regression tasks for PV module quality assessment 	

**Fig. 7.** Machine learning-based defect detection (reproduced from [20] with permission).

cell area. Further, using distributed diode model (Fig. 4 (d)) locally resolved power loss can also be determined. Eq. (7) shows the estimation of local $R_{s(i)}$ from local voltage drop ($\Delta V_{R_s(i)}$) and local current ($I_{EL(i)}$) in a simplified case [84].

$$R_{s(i)} = \frac{\Delta V_{R_s(i)}}{I_{EL(i)}} \quad (7)$$

Similar mapping of spatially resolved parameters such as I_{01} , n_1 , R_{sh} has been demonstrated by [10,75] from the EL images.

Fuyuki et al. [31] have shown the estimation of cell ideality factor (n_1) using the slope a cell EL current-intensity response for the estimation of cell lumped parameters. This work has estimated cell V_{oc} with respect to reference cell with known parameters using Eq. (8) derived from Eq. (2).

$$\phi_{EL(test)} = \exp\left(\frac{V_{oc(test)} - V_{oc(ref)}}{V_i}\right) \quad (8)$$

For the estimation of lumped parameter of a cell, average cell ϕ_{EL} or intensity of brightest point near busbar is used. Potthoff et al. [66] have

estimated the cell voltages (Fig. 8(b)) within a module using Eq. (3). Using low and high bias EL images, module cumulative series resistance (R_{mod}) as well as average cell R_s can also be estimated (Eq. (9)) taking the difference between measured module terminal voltage (V_{mod}) and summation of estimated cell voltages dividing EL current and total number of cells in a module (N).

$$R_{cell(average)} = \frac{V_{mod} - \sum V_i \log\left(\frac{\phi_{EL}}{A}\right)}{NI_{EL}} \quad (9)$$

Roy and Gupta [75] have proposed an iterative method for the quantitative estimation of ohmic shunts within a cell. Local value of R_{sh} is estimated using Eq. (10). In this method, voltage across ohmic shunt (V_{Rsh}) is estimated using Eq. (3), current flowing through it (I_{Rsh}) is estimated from iterative simulation.

$$R_{sh} = \frac{V_{Rsh}}{I_{Rsh}} \quad (10)$$

3.2. Module level quantitative EL imaging

Cell or sub-cell level quantification is useful at production line or laboratory research. For the evaluation of field-operational module performance, module level quantitative EL assessment is required. In this Section, review of state-of-the-art quantitative EL methods reported for different types of defects and degradations is presented. Fig. 9 show the overview of quantitative EL methods discussed in this Section. Methods discussed in Section 3.2.1–3.2.3 quantifies the impact of particular type of defects and degradations. The methods discussed in Section 3.2.4 are applicable to a module with multiple defects and degradation.

3.2.1. Quantitative evaluation of optical defects and degradations

In this section, quantitative EL methods for evaluating the impact of cell breakages and soiling are presented.

3.2.1.1. Quantification of cell breakages impact. Castañeda et al. [13] have made first attempt to quantify performance loss due to cell breakages (mode C cracks) from an EL image. In this work, active area of

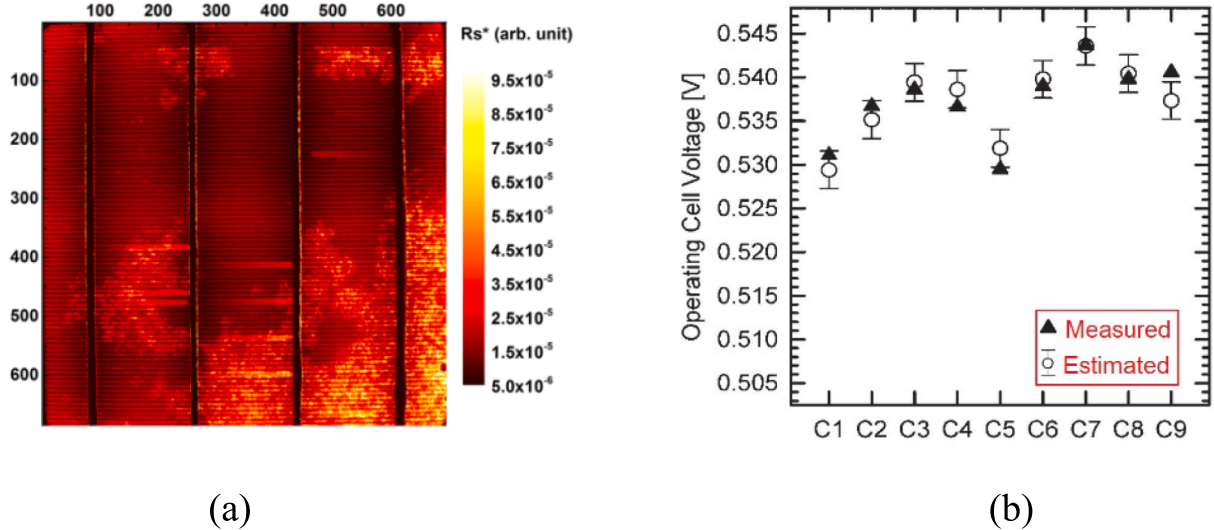


Fig. 8. (a) Spatially resolved R_s map of a c-Si cell (reproduced from [62] with permission) (b) Estimated and measured cell voltages of the cells within a packed module (reproduced from [66]).

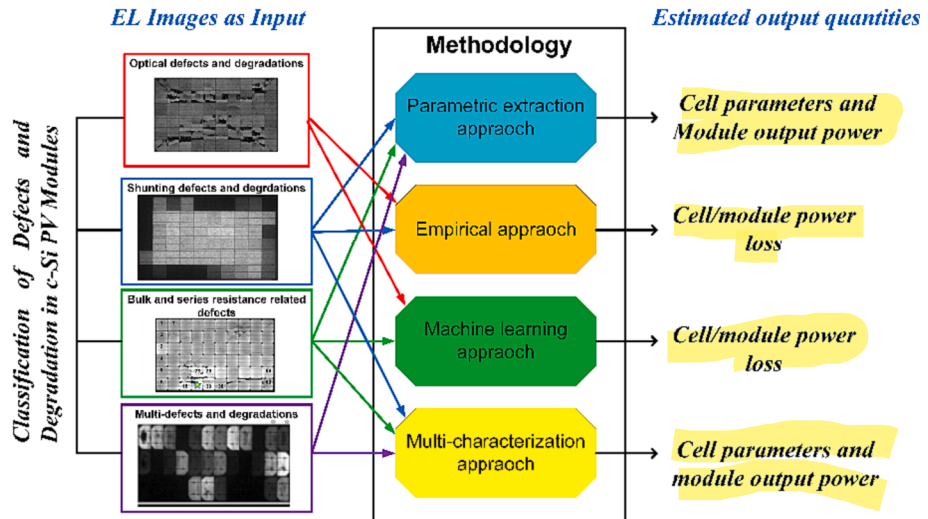


Fig. 9. Overview of EL imaging-based quantitative assessment of various defects and degradations.

a cracked cell is statistically calculated from an EL image. Further, based on the calculated active area, ideal I_{sc} of cracked cell was calculated using nameplate I_{sc} , (Ideal I_{sc} = nameplate I_{sc} rating \times normalized active area). For estimating actual I_{sc} of a cracked cell, QE were used to estimate current density of active area i.e., Actual I_{sc} = Current density \times active cell area. By comparing Ideal I_{sc} and Actual I_{sc} , cell I_{sc} loss due to

cracked is estimated. It was shown that cell isolation due to crack causes I_{sc} loss proportional to inactive area, which is quite logical. However, this work was only able to find I_{sc} loss due to cell breakages without providing an approach for quantifying module level impact of cell breakages.

Rodrigues et al. [74], in true sense quantified the impact of cell

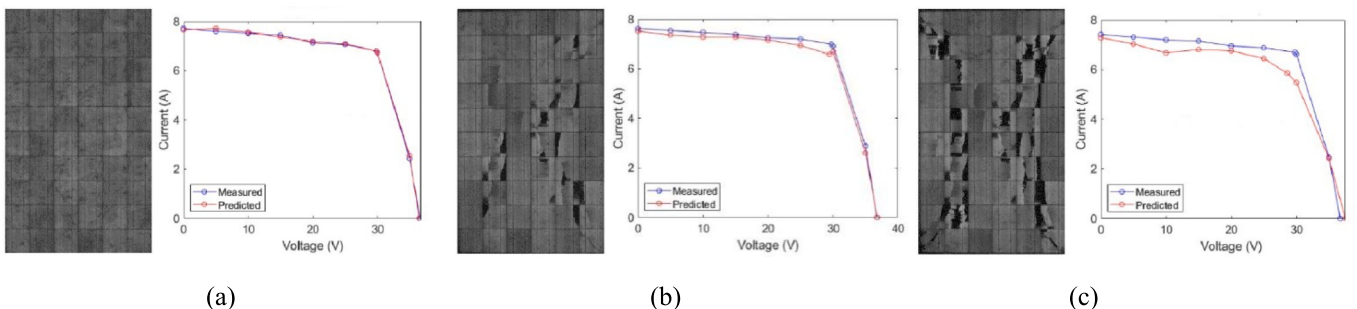


Fig. 10. (a) Healthy module (b) Module with moderate cell breakages (c) Module with severe cell breakages (reproduced from [74]).

breakages on module output. The deep learning approach have been used to predict $I-V$ curve of a module with inactive cell area as dominant fault from the EL images. Large number of EL images were acquired from different modules with cell breakages showing complete dark appearance in EL images (see Fig. 10). The deep learning models were trained and verified based on the captured EL data. 11 models were developed (I_{sc} , Current@5V, Current@10 V, Current@15 V, Current@20 V, Current@25 V, Current@30 V, Current@35 V, Imp_p, V_{mpp}, V_{oc}). Fig. 10 show the EL images of the test modules and corresponding $I-V$ generated by the proposed deep learning method. In case of mild and moderate form of cell isolation, generated $I-V$ curve shows close appearance and less relative error at MPP. However, in the severely defective module, relative error is quite high (about 16 %) i.e., accuracy of the prediction decreases as severity of defect increases. The possible reason behind largest error may be the used training data set might contain lesser number of severely cracked modules as severe form of cell breakages is not common pattern. Results highlight the potential of the proposed models as power prediction is based on only single EL image without other measurements. Although, future work is required to improve prediction accuracy for a severe form of cell breakages possible by training ML models based larger data set of modules with moderate to severe form of cell breakages.

3.2.1.2. Evaluation of soiling power loss. Doll et al. [23] have explored the use of EL imaging to detect, characterize and quantify soiling losses from the EL images. Module average EL intensity reduction ($\phi_{EL,loss}$) due to soiling is calculated by subtracting EL images taken before and after the soiling. Based on calculated ($\phi_{EL,loss}$), module P_{loss} due to soiling estimated using Eq. (11). The correlation constant/factor (C_f) was determined from the available test module $I-V$ data.

$$\text{Module } P_{loss} = C_f \cdot \phi_{EL,loss} \quad (11)$$

In Fig. 11 (a), the subtracted EL image shows $\phi_{EL,loss}$ due to soiling. Estimated soiling power loss show about 2% relative error with respect to measured STC power loss as shown in Fig. 11 (b).

The necessary condition before applying Eq. (11) is to ensure $\phi_{EL,loss}$ is not due to shunting or other defects. Although the proposed correlation is simple and easy to use, it is based on the study of only five module. Hence, future work is required to generalize and consolidate the

proposed linear relationship between $\phi_{EL,loss}$ and soiling power loss with large data set consisting of different possible soft to hard soiling patterns normally observed in a field.

3.2.2. Quantification of bulk diode and series resistance related defects and degradations

This section presents the quantitative EL methods for evaluating defects affecting bulk semiconductor properties (LID, LeTID) and series resistance (corrosion, finger breakage, cell cracks).

3.2.2.1. Extraction of pristine PV module parameters. This paper [29] has shown the first time use of EL images for the estimation of parameters I_{01}, I_{02} , and n_1, n_2 of an individual PV cell within a module in non-destructive manner. Voltage dependent EL imaging along with module $I-V$ curve were used to estimate parameters, in which I_{01} and n_1 extracted using logarithmic relation of ratio of cell ϕ_{EL} with applied I_{EL} using Eq. (12). Further individual cell parameters I_{02}, n_2 were derived by fitting.

$$\log\left(\frac{\phi_{test}}{\phi_{ref}}\right) = \log\frac{A_{test}}{A_{ref}} + \log\left(\frac{I_{01,test}^{n_1,test}}{I_{01,ref}^{n_1,ref}}\right) + (n_1_{test} - n_1_{ref}) \cdot \log(I_{EL}) \quad (12)$$

Approach was validated on small test module consist of four cell. Average relative error in estimation of I_{01} , n_1 , I_{02} , n_2 was observed as 21.2%, 0.8%, 23.2%, and 4.1%, respectively, which may cause cumulative error around 2 to 3% in the estimation of P_{out} . The proposed approach has been tested on pristine module only. Also, extending its use to a commercial size module with high number of cells would be difficult as it involves use of Eq. (12) and manual derivation of I_{02}, n_2 by fitting for an individual cell.

3.2.2.2. Quantification of LID and finger breakage impact. Rajput et al. [71] have proposed analytical approaches to evaluate the impact of degradations on cell I_{01} and R_s parameters. In this method, two EL images were used for the analysis captured at high (I_{sc}) and low EL current ($0.2I_{sc}$). Further based on the EL images, solution of spatial analytical EL equations conducted to generate map of cell I_{01} and R_s as shown in Fig. 12 (b) and (c), respectively. Based on the estimated cell parameters, SDM is simulated to quantify module P_{out} by generating $I-V$ curve. Fig. 12(d) shows the simulated $I-V$ characteristics of the defective cell

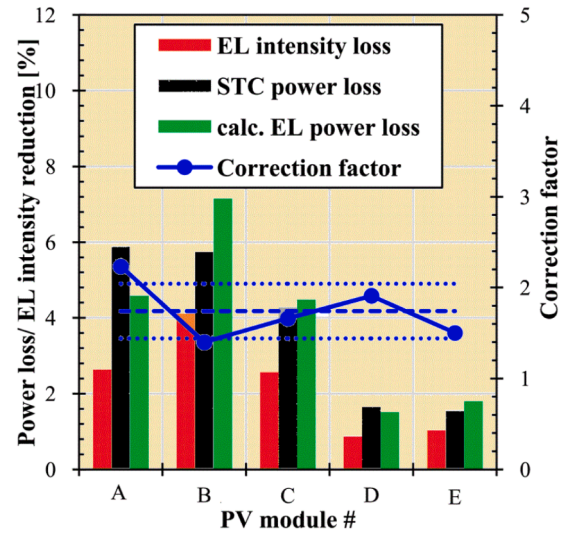
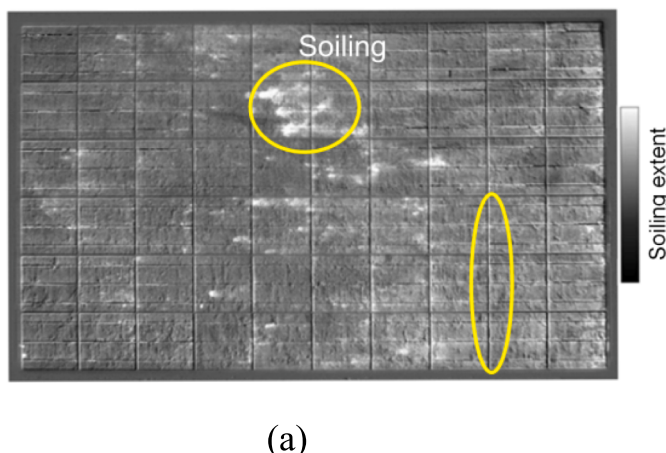


Fig. 11. (a) Subtracted EL image showing soiling extent (b) Calculated EL intensity loss and estimated soiling power loss for test modules (reproduced from [23]).

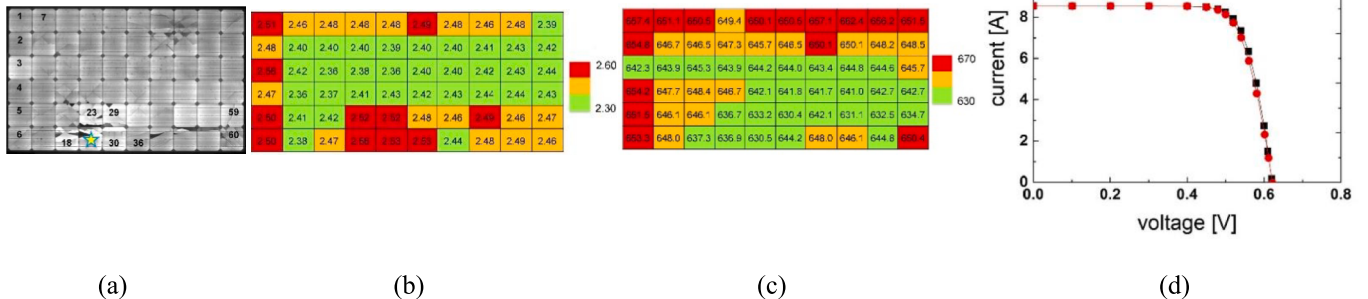


Fig. 12. (a) EL image of the test module (b) cell R_s map (c) cell I_{01} map (d) comparison of simulated I - V curve before and after the cell correction (reproduced from [71] with permission).

(marked by star in Fig. 12(a)). The authors have estimated defective cell R_s and I_{01} parameters and simulated cell performance using SDM. The generated I - V curve is referred as before correction in Fig. 12(d). Further, to see the drop in performance due to the defect, I_{01} and R_s parameters of the defective cell have been replaced with average values of I_{01} and R_s based on other healthy cells within the module. The simulated I - V curve generated based on healthy cell average parameters I_{01} and R_s has been referred to as after correction in Fig. 12(d) so that the comparison of these two I - V characteristics gives performance loss attributed by cell defect.

Further, in [72], the proposed methods strongly validated for outdoor condition, by capturing EL images by Si-CCD and InGaAs camera in night as well as daylight. Result (Fig. 12 (d)) shows the merit of the proposed method to accurately generate module I - V curve with relative error $< 3\%$ in P_{out} . In simulation, n_1 and R_{sh} are assumed to be 1 and 1000Ω , respectively. It implies that in presence of degradation that affects R_{sh} or n_1 this approach is not directly applicable. Also, this method estimates cell internal R_s , in future may be the combination of this method with [66] work would enable the evaluation of defects (busbar interconnect failure, corrosion) affecting external R_s also, which may not be visible in EL images.

3.2.2.3. Quantification of cell cracks in PV module. Kropp et al. [51] have estimated P_{loss} of hail damaged PV module (Mode B cracks). This method also uses two EL images of defective module for the quantification captured at high ($>0.3I_{sc}$) and low current ($0.1I_{sc}$). For the analysis, it was assumed that mechanical cracks solely change cell R_s . Using two EL images, R_s map of a PV module was estimated by solving analytical equations. Further, based on estimated cell R_s map and datasheet information (extracting I_{01} , n_1 parameters), SDM simulations is performed to estimate module P_{out} by generating I - V curve. Fig. 13 show the result of this work, authors have shown that proposed approach estimates module P_{out} with relative error $< 4.3\%$. On limitation side, this approach requires cell constants like I_{01} and n_1 which need to be determined from module datasheet. In case of field-aged modules, I_{01} and n_1 parameters cannot be taken from module datasheet since they may differ from actual values due to ageing. Hence, for good accuracy this method is applicable for evaluating cracks in newly installed or unaged PV modules where required auxiliary parameters can be taken from a module datasheet.

3.2.2.4. Quantification of corrosion impact. Karimi et al. [46] have predicted the module power and R_s degradation from EL images using ML approach. The proposed methods use various EL pixel intensity-based features and classifies the cell-level images based on extent of corrosion (Fig. 14(a)) using convolutional neural network. Calculating module-level corrosion index based on cell classes, four polynomial regression models (Median intensity, Fraction of dark pixels,

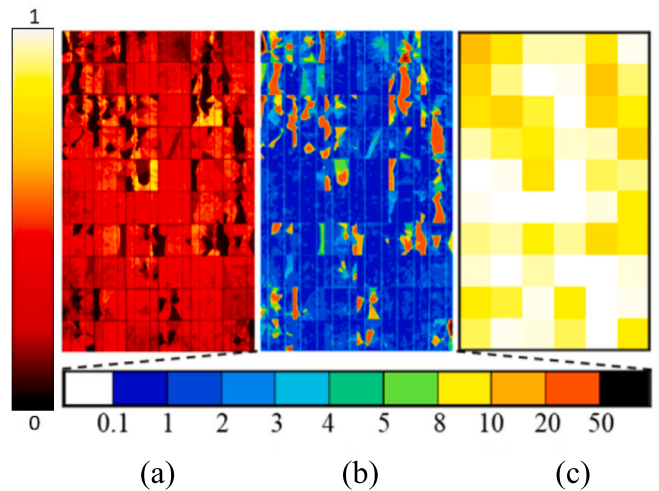


Fig. 13. (a) EL image of the test module (b) Estimated R_s map (c) Estimated cell power map (reproduced from [51]).

Normalized busbar width and Busbar corrosion ratio) have been built to predict P_{out} and R_s . Fig. 14 show the results of model Busbar corrosion ratio (F_{BBCR}) which quantifies the busbar level corrosion from cell level EL images. Fig. 14(b) and (c) show the normalized R_s and P_{out} estimated for test modules belonging to three different brands with high confidence and an adjusted-R² of 0.73 and 0.81, respectively. The proposed model requires initial EL images and I - V data to estimate module output from the EL images throughout the module lifespan.

3.2.3. Quantification of shunting defects and degradations

This section presents the different quantitative EL methods for analyzing shunting defects and degradation, mainly PID-s.

3.2.3.1. Quantitative EL analysis (QELA) method. Bedrich et al. [6] firstly reported an empirical approach for the quantification of PID-s losses. This method uses two EL images of attest module taken either at two different EL currents or before/after degradation. Taking the logarithmic ratio of two EL images, spatially resolved PID-s P_{loss} is estimated using Eq. (13), where f is correlation constant, it depends on the size and number of cells, cell technology and series resistance.

$$\Delta P_{loss}(i,j) = f V_{th} \log\left(\frac{\phi_{after}(i,j)}{\phi_{before}(i,j)}\right) \bullet 100\% \quad (13)$$

Fig. 15 (a) shows the spatially resolved power loss within an individual cell of the PID-s module estimated using Eq. (13). Fig. 15 (b)

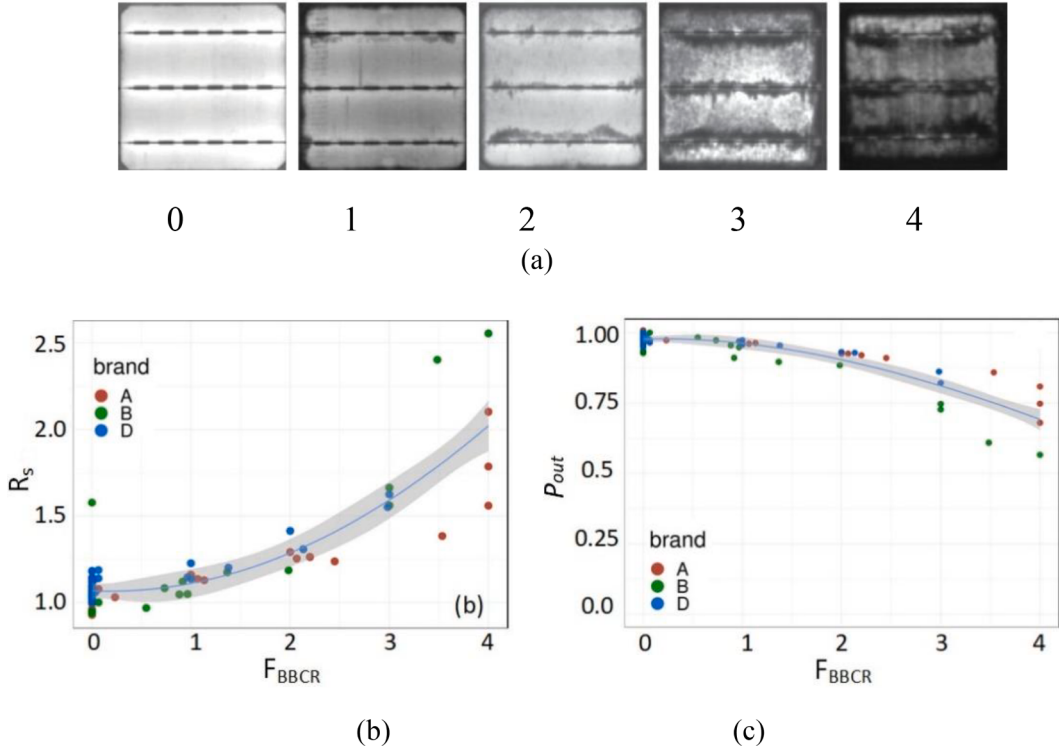


Fig. 14. (a) EL images of cells labeled into five level of busbar darkening in increasing order of corrosion from 0 to 4 (b) Normalized R_s prediction by F_{BBCR} model for three brands of test modules (c) Normalized P_{out} predicted by F_{BBCR} model for three brands of test modules (reproduced from [46]).

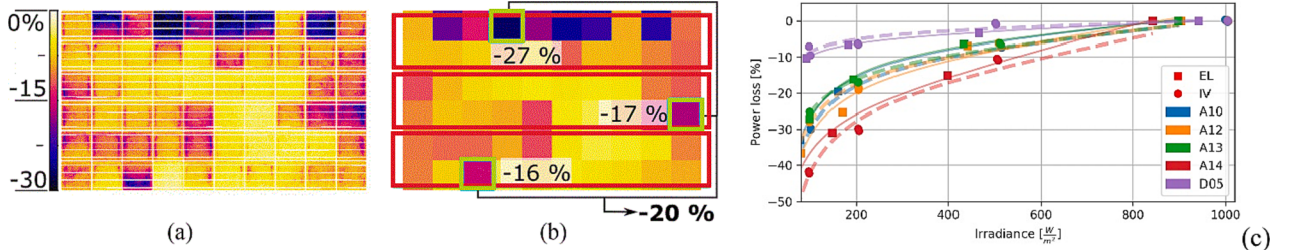


Fig. 15. (a) Spatially resolved power loss map (b) Cell average power loss map (c) Comparison of power loss of test modules at different irradiances (solid lines: fitted EL; dashed line: $I\text{-}V$ points) (reproduced from [6]).

shows an individual cell average power loss calculated by averaging spatially resolved power loss in Fig. 15 (a). Further, module power loss has been calculated by taking average of worst performing cell per string, which figure out as -20% in Fig. 15 (b). This method has been strongly validated based on the analysis of 2000 EL images. Apart from estimating STC power loss, this work also provides the correlation for predicting power losses at other operating conditions (Fig. 15(c)) using 2–3 EL images captured at currents equivalent to the desired irradiances. Fig. 15(c) shows that RMSE remains $<3\%$ between measured and predicted data points by $I\text{-}V$ and EL method, respectively. On limitation side, this method requires the determination of module-specific correlation constant, which may require module terminal measurements.

3.2.3.2. EL power prediction of module (ELMO) method. Kropp et al. [51] have developed ELMO method in which analytical approach is used for the estimation of P_{out} of a PID-s module. This method uses single low current EL image for the estimation of cell R_{sh} . Using single EL images, Eq. (14) estimates R_{sh} map of a PV module. Further, based on the estimated values of cell R_{sh} , SDM is simulated to find module P_{out} . Fig. 16 (a) shows the low current EL image of a test module and a corresponding estimated cell power map in Fig. 16 (b).

$$R_{sh(i)} = \frac{n_1 V_i \log(\phi_i)}{I_{EL} - I_{0i} \phi_i} \quad (14)$$

$R_{sh(i)}$ – Shunt resistance of i^{th} cell, A – voltage calibration constant, ϕ_i – EL intensity of i^{th} cell.

This method uses single low current EL image captured with EL current $< 0.1I_{sc}$. In case of PID-s, as its severity increases, low current EL images saturates i.e. no EL emission results from a PID-s cell at lower current (see Fig. 5(d)). Since shunt defects sinks significant EL current, negligible current flows through bulk $p\text{-}n$ junction diode which is responsible for EL emission. Hence, this method is applicable for evaluating the early phase of PID-s or weak ohmic shunts only.

3.2.3.3. Standardized EL methods. Standardized EL method have been proposed by Puranik and Gupta [67] for qualitative and quantitative investigation of PID-s. In this method, two EL images captured at low and high EL current have been used for investigation. Ratio of two EL images captured at $0.2I_{sc}$ and I_{sc} is taken as PID-s index ($C_{\phi EL}$) to represent shunting, i.e., cell PID-s index ($C_{\phi EL}$) = $\phi_{EL(0.2I_{sc})}/\phi_{EL(I_{sc})}$. For PID-s detection, cell PID-s indices further compared with PID-s threshold, which has been derived equivalent to 5% power loss

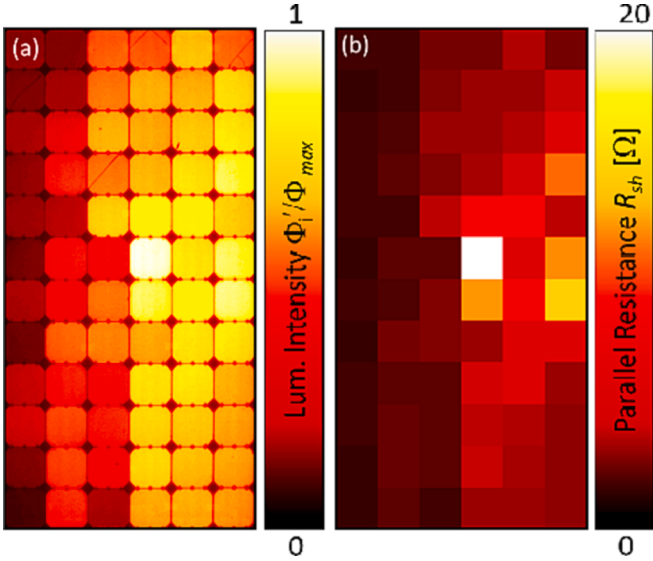


Fig. 16. (a) Low current ($<0.1I_{sc}$) EL image of a test module (b) Estimated R_{sh} map of a PID-s module (reproduced from [51]).

qualification criterion of IEC TS 62804–1 [39]. This method was called as standardized as it has been developed considering the parameters equivalent to IEC standards for efficient PID-s investigation.

Fig. 17 shows the comparison of cell PID-s indices and PID threshold, as per this method cell with $\text{PID-s index} \leq \text{PID-s threshold}$ qualifies for PID-s and magnitude of PID-s index reflects severity of PID-s. This paper has further derived an empirical correlation (Eq. (15)), relating normalized cell P_{loss} as a function of PID-s index. For quantification, this individual cell PID-s indices can be calculated by taking ratio of two EL images ($0.2I_{sc}$ and I_{sc}). Further, based on cell PID-s index, PID-s power loss of each cell can be predicted using Eq. (15).

$$P_{loss}(\%) = 0.09C_{\phi_{EL}}^2(\%) - 2.80C_{\phi_{EL}}(\%) + 24 \quad (15)$$

Fig. 18 show that, the proposed correlation estimates cell power loss with relative error less than $<\pm 3\%$. The Eq. (15) is free from any module specific constant. Also, only ratio of two EL images is required which makes its application simple in field conditions. However, this work does not show estimation of module level power loss based on estimated cell power losses. Also, unlike QELA [6] this does not predict power losses at other operating conditions apart from STC condition. Future work may be conducted to overcome the existing limitations following similar approach to [6].

3.2.3.4. Novel quantitative electroluminescence (QUEL) method. Puranik and Gupta [69] have proposed novel QUEL method for the detailed cell level performance evaluation of PID-s module. The QUEL has been developed based on the analysis of EL characteristics ($I_{EL}\phi_{EL}$ and $V\phi_{EL}$)

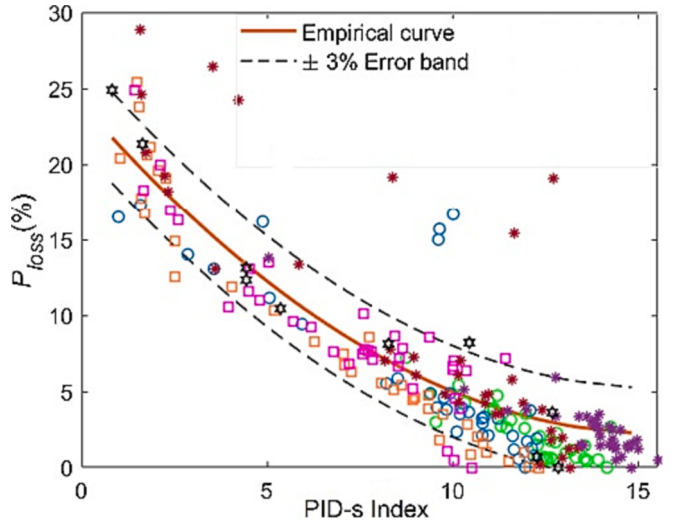


Fig. 18. Plot of cell PID-s index Vs cell P_{loss} (reproduced from [67] with permission).

of a PID-s cell. In this method, multiple EL images (>4) have been used for the quantification captured at different EL current. From the input EL images, QUEL algorithm extracts seven parameters ($I_{ph}, I_{01}, n_1, I_{02}, n_2, R_s, R_{sh}$) of the cells in step-wise manner, solving number of equations. This method estimates I_{ph} equating with module datasheet I_{sc} as it is not affected by PID-s. Further, this method estimates EL calibration constant A, A'' and n_1 from the $I_{EL}\phi_{EL}$ and $V\phi_{EL}$ characteristics. Extraction of A, A'' and n_1 further enables the estimation of I_{01} and R_s using Eq. (5) and Eq. (9), respectively. For the determination of shunt parameters (I_{02}, n_2, R_{sh}), this method solves a set of three non-linear equations. Further, based on the extracted cell parameters, simulations are performed to estimate module P_{out} by generating module $I-V$ curve. Fig. 19 shows the cell and module level results of the QUEL method. The use of $I_{EL}\phi_{EL}$ characteristics enables QUEL method to evaluate a PID-s cell performance in a contact-less manner. The proposed method estimates cell or module P_{out} relative error $<\pm 3\%$.

Major limitation of the QUEL method is that severely PID-s/shunted cell cannot be evaluated since severe PID-s cell does not emit active EL emission for the practical range of $I_{EL} \leq I_{sc}$ or $1.3 \cdot I_{sc}$, which is discussed in more detail in (Puranik and Gupta, [68,69]).

3.2.4. Quantitative EL methods for evaluating multi-defects and degradations

In Section 3.2.1–3.2.3, presented quantitative EL methods evaluates specific type of defects and degradations. However, multiple coexisting defects and degradations exist in a field operational module served for longer duration. Hence, it is essential to consider different class of coexisting defect and degradations in quantification. From that view,

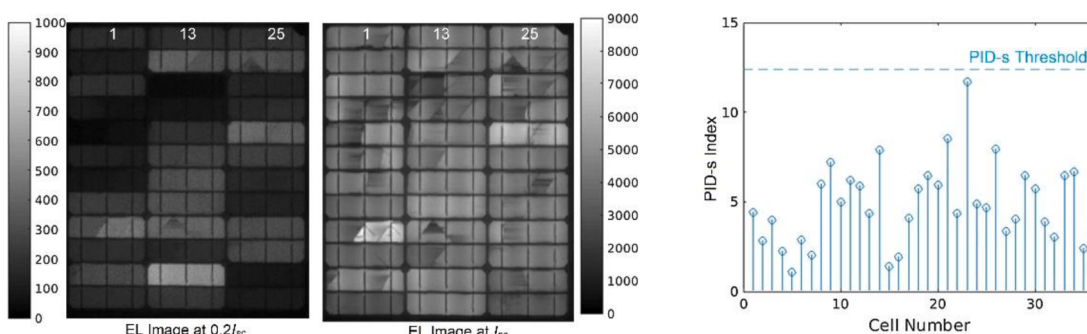


Fig. 17. PID-s investigation using ratio of EL intensities (reproduced from [67] with permission).

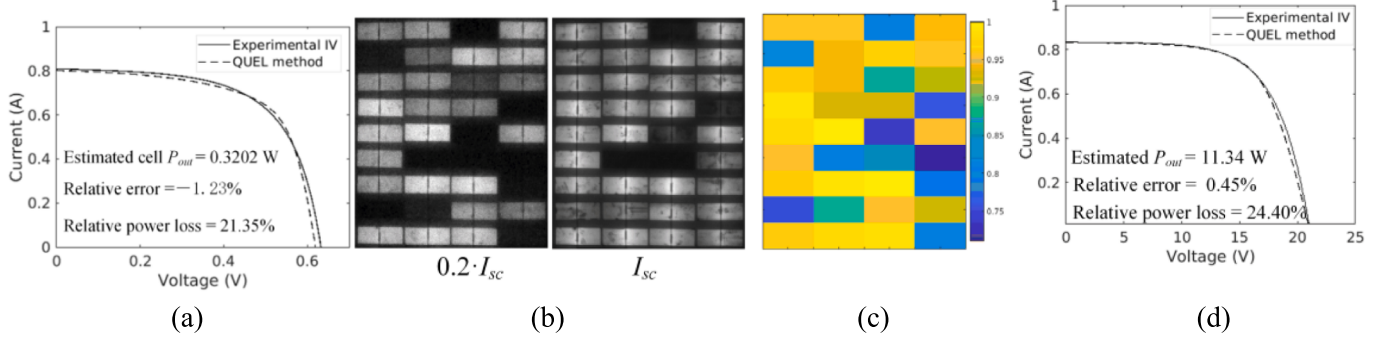


Fig. 19. (a) PID-s cell results (b) EL images of the test module (c) Cell power map (d) PID-s module results (reproduced from [69] with permission).

researchers have reported some quantitative EL methods, which are discussed in this section.

3.2.4.1. Quantification using EL-DLIT techniques. Bauer et al. [3] have used the combination of EL imaging and dark lock in thermography (DLIT) to obtain an individual cell I - V characteristic. Cell operating voltages and R_s estimated following the approach similar to [66] (Eq. (8) and Eq. (9)) as discussed in Section 3.1. At the estimated voltages, DLIT quadrature phase images taken in forward bias condition were used for local I - V evaluation [8–9]. Fig. 20(a) and (b) show the estimated cell power map and I - V curves of the few test cells. Results shows that this approach estimates cell, and module P_{out} with relative error < 2% and provides detailed performance analysis. Combined EL-DLIT analysis enables detailed cell/sub-cell level quantitative analysis due to the advantage of EL imaging for local voltage estimation and DLIT for local current mapping. However, use of DLIT limits the applicability of this approach to laboratory analysis of degradation only due to high capturing time and expensive DLIT set up.

3.2.4.2. Quantification using EL-IV measurements. Dix-Peek et al. [22] have combined injection-dependent EL imaging with module dark I - V characteristics to determine individual cell characteristic in non-destructive manner. Using the approach similar to [66], this method estimates an individual cell voltage from the captured EL images at different EL current to generated cell dark I - V characteristic. From dark I - V curve, cell parameters were estimated with a preliminary assumption of R_{sh} value. Further using individual cell I - V parameters along with complete module dark I - V data, R_{sh} was re-optimized using genetic algorithm. Cell level dark I - V and module level light I - V were simulated assuming same value of I_{ph} for all the cells. The proposed method allows to estimate MPP at different irradiance as shown in Fig. 21. The requirement of module I - V measurement restricts the applicability of the proposed method to indoor degradation analysis.

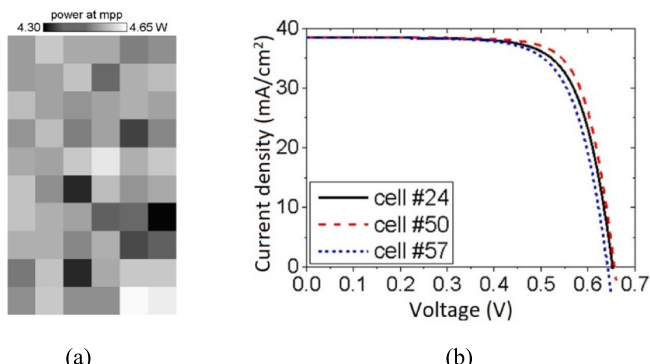


Fig. 20. (a) Estimated cell power map (b) Generated I - V characteristics of the test cells (reproduced from [3] with permission).

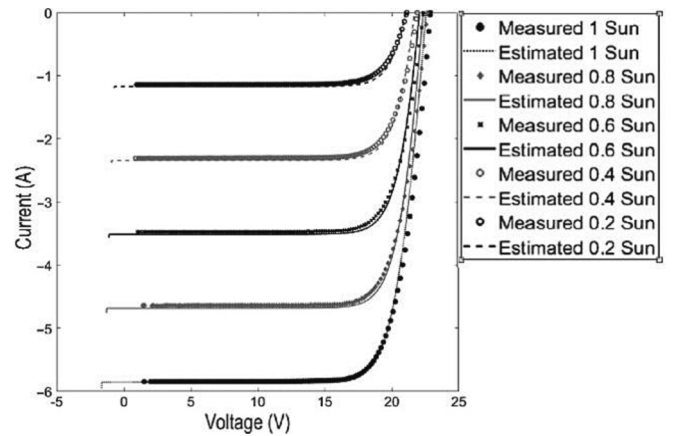


Fig. 21. Comparison of experimental and simulated I - V characteristics at different irradiance (reproduced from [22]).

3.2.4.3. EL sweep method. In I - V measurements, a module is biased by a variable voltage source ($0, V_{oc}$) and resulting current is measured to generate I - V curve. Similarly, the EL sweep method has been introduced by [15]. This method uses 6 to 15 EL images of a test module captured at different EL current. From the input EL images, cell voltages (V_{op}^n) are calculated using Eq. (16) for each applied EL current. Further, using pair of applied EL current and estimated cell voltage dark I - V curve of each cell can be constructed.

$$V_{op}^n = V_{mod} \log(\phi_{max}(i,j)) + \frac{V_{mod} - \sum V_i \log(\phi_{max}^n(i,j))}{N} \quad (16)$$

In the conventional approach of estimating cell voltages using Eq. (3) [66]), determination of voltage calibration constant (A) is essential, which requires module terminal voltage measurements at low biasing level ($\leq 0.1I_{sc}$). In that comparison, Eq. (16) does not contain any calibration constant term; hence, in the EL sweep method provides quantitative analysis without requiring module calibration. From the obtained cell I - V characteristic, cell parameters can be extracted using curve fitting method further to generate module I - V curve by modeling and simulation. This work has analyzed impact of different imaging parameters, camera technology, and environment on the performance of the EL sweep method. Results (Fig. 22) have shown that the EL sweep method can generate cell I - V curve non-contact manner with RMSE < 0.01.

This method has limited applicability to a weak or non-shunted module. In case of shunted cell (PID-s affected module) I - V curve points in low voltage region cannot be estimated due to non-emission of EL signal and poor signal-to-noise ratio.

3.2.4.4. Generalized quantitative EL (g-QUEL) method.

Puranik et al.

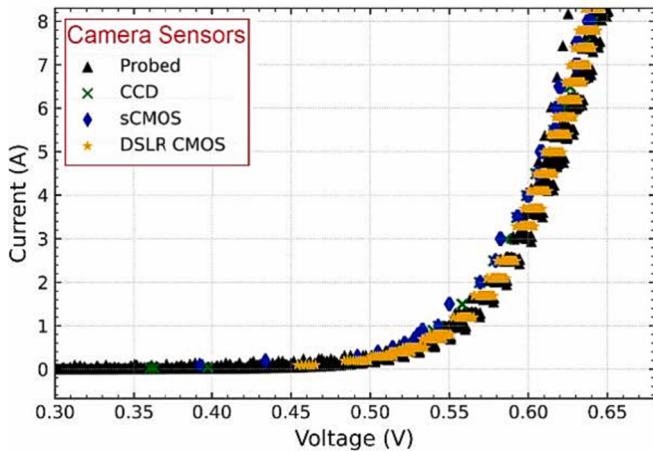


Fig. 22. Cell dark I - V obtained using EL sweep method (reproduced from [15] with permission).

[70] have proposed generalized QUEL (g -QUEL) method, which is the extension of novel QUEL method discussed in Section 3.2.3.4. The g -QUEL method quantifies multiple coexisting defects and degradation, excluding optical defects and degradations. The knowledge of EL characteristics I_{EL} - ϕ_{EL} and V - ϕ_{EL} for different types of defects and degradation have been used in building g -QUEL method. Similar to QUEL method (Section 3.2.3.4), the g -QUEL method uses multiple EL images of a test module captured at different EL currents for the quantification. From the input EL images (4 to 10), this method extracts five/seven parameters in step-wise manner. Further, based on the extracted parameters module simulation are performed at sub-module or cell level for the estimation of module P_{out} by generating module I - V curve.

Results (Fig. 23) shows that the g -QUEL method evaluates module performance with relative error $< \pm 3\text{-}5\%$. On limitations, it could not quantify severely degraded shunted module due to non-emitting cells (as discussed in Section 3.2.3). Also, some steps of the g -QUEL method requiring manual intervention make it complex to implement, which may be automated in the future.

4. Summary and comparison of quantification techniques

The module level quantitative EL methods are summarized in point-wise manner in Table 4. The first two columns of Table 4 show the four categories of defects and degradations and the corresponding literature discussed in Section 3.2.1 to 3.2.4. The contribution of each paper is assessed based on the input requirements (number of EL images and other auxiliary measurements), proposed approach (parametric extraction, machine learning, empirical), and performance of quantification (cell/module P_{out} , other internal parameters). The findings of the assessment are presented in separate columns in the form of key

outcomes, merits, demerits, applications, and limitations. Indoor and outdoor applicability of each method is judged based on the requirement of input measurements. In indoor conditions (laboratory research or production line), it is possible to capture high number of EL images and conduct different types of measurements, such as I - V , DLIT, or QE, in a controlled environment. Hence, all methods have default applicability for indoor conditions. In outdoor conditions considering the assessment of operational module in a large PV field, some techniques are not feasible to perform such as DLIT, QE or number of I - V measurements at individual module level. In the last column, the scope of future work and possible field application challenges of each work are highlighted.

5. Discussion and future scope

Table 4 provides a detailed summary of progress in quantitative EL imaging. Most methods can be useful in outdoor conditions for evaluating performance of a module operating in a large PV field, where it is essential to monitor the performance of a module for the economic operation of a plant. From that view, the conventional use of I - V is cumbersome, involves manual intervention, and tedious for large PV field. From that view, quantitative EL methods can enable detailed short-term and long-term performance analysis of field-operational modules from captured EL images. The quantitative EL methods can facilitate evaluating impact of existing defects and degradations and taking appropriate corrective measures to optimize plant performance. This section presents a detailed discussion and future scope of development in module level quantitative EL imaging for each class of defects and degradations mentioned in Section 3.2.1 to 3.2.4.

5.1. Optical defects and degradations

Quantification of optical issues, mainly cell breakages and soiling, have been discussed in the literature. In cell breakages, part of a cell is completely disconnected and does not contribute to current generation, which is easy to determine from an EL image. However, in discoloration, soiling, or moisture ingress, defective area gets partially shaded rather than complete electrical disconnection. Hence, unlike other cell parameters, estimation of current generation or I_{sc} loss of a defective cell from sole EL images is quite difficult. In that case, QE analysis would be useful in developing future quantitative EL methods for I_{ph} -related issues, as shown by [13].

- Although the reported quantitative EL work for optical defects and degradation is lesser than others, [74] and [23] show the good potential of EL imaging in evaluating the impact of optical defects.
- There is scope of future work for developing quantitative EL methods for major degradations such as discoloration, hard soiling, and delamination, which are prevalent after 10–12 years of module field operation.

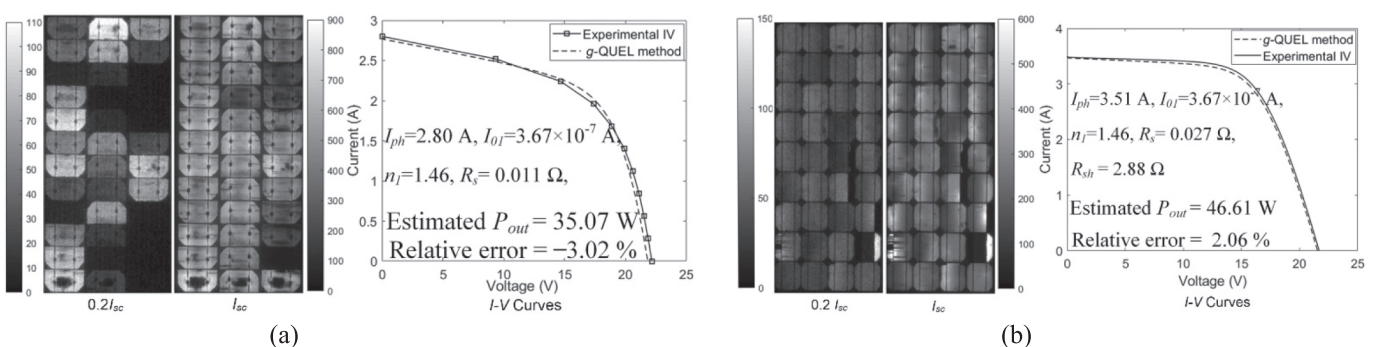


Fig. 23. Experimental results of the field aged (a) shunted (b) non-shunted module (reproduced from [70] with permission).

Table 4

Detailed summary of the quantitative EL methods.

Literature	Defect and degradation possible to evaluate	Required number of EL images with biasing level, number of PV modules used and other measurements	Approach	Output quantities	Key outcome, Merits and Applicability	Demerits, Limitations and other complexity	Future scope and field application challenges
Optical defects and degradations	[13]	• Cell breakages (Mode C cracks)	• Single EL image captured at I_{sc} • 1 module	Simple analytical equations <ul style="list-style-type: none"> Calculated active area of cracked cell from an EL image Cell ideal I_{sc} was calculated by multiplying nameplate I_{sc} with normalized active area Cell actual I_{sc} estimated from current density (determined by QE) multiplying with active cell area Estimated cell I_{sc} loss by comparing cell ideal and actual I_{sc} 	• I_{sc} loss <ul style="list-style-type: none"> Useful for simple calculation of active/inactive cell area and resulted I_{sc} loss from single EL image Indoor application 	<ul style="list-style-type: none"> This work does not give any clear idea of module P_{loss} caused by cell breakages. Also estimation of I_{sc} loss is not useful in presence of other defect. Requirement of QE for estimating I_{sc} of cell/module makes it almost impossible to use in field 	<ul style="list-style-type: none"> Further work is required to develop an approach to estimate P_{loss} due to inhomogeneous cell breakages from an EL image also making it field usable
	[74]	• Cell isolated areas (Mode C cracks)	• Single EL image captured at I_{sc} • 10 modules	Deep learning algorithms <ul style="list-style-type: none"> Captured large set of EL images of the modules with cell breakages EL data used for training eleven deep learning models Trained models predicts 10 points including I_{sc}, MPP and V_{oc} of I-V curve from an EL image 	• P_{out} (Module) <ul style="list-style-type: none"> Proposed models shows satisfactory performance of predicting module P_{out} based on single EL image only It would be useful for analyzing field operational cracked module as it require only single EL image without any other information Outdoor application 	<ul style="list-style-type: none"> Accuracy decreases as defect (cell isolation) severity increase within a module (relative error $\sim 16\%$ for severe defect). Proposed models are insensitive in presence of other defects 	<ul style="list-style-type: none"> Need to improve accuracy for severely defective modules possibly by training deep learning models with larger data set More consolidation and detail error analysis is required For making it robust and generalized, data set used in training should contain modules from different manufacture and cell size, type, and technology
	[23]	• Soiling	• Two EL images of a test module taken before and after soiling captured at $0.9I_{sc}$ • 5 modules • Some I-V data for estimation of calibration factor	Simple empirical correlation <ul style="list-style-type: none"> Module average EL intensity reduction (ϕ_{EL}) due to soiling is calculated by subtracting EL images taken before and after the soiling Eq. (8) used for estimating soiling P_{loss} from calculated (ϕ_{EL}) 	• P_{loss} (Module) <ul style="list-style-type: none"> Paper have shown that quantification of P_{loss} due to soiling is possible from EL images with relative error $< 2\%$ Correlation is simple and can be used for field applications for fully automated quantification of soiling loss from captured EL images Outdoor application 	<ul style="list-style-type: none"> Need timely taken EL images in which pixel-by-pixel subtraction is difficult. Outdoor EL images may require more image processing For the determination of empirical factor module I-V measurements are required Currently not generalized and based on small data set (five modules only) 	<ul style="list-style-type: none"> Detailed study is required considering different soiling pattern to prove linear and generalized relationship between soiling power loss and EL intensity loss. In field application, key challenge is taking two images at different time instances and bringing them to same reference frame for pixel by pixel image subtraction

(continued on next page)

Table 4 (continued)

Literature	Defect and degradation possible to evaluate	Required number of EL images with biasing level, number of PV modules used and other measurements	Approach	Output quantities	Key outcome, Merits and Applicability	Demerits, Limitations and other complexity	Future scope and field application challenges	
Bulk and series resistance related defects and degradations	[29]	Healthy cell/module	<ul style="list-style-type: none"> 13–15 EL images captured at cell voltage biasing between 0.3 and 0.65 V 1 module Module I-V curve 	<ul style="list-style-type: none"> Analytical equations and curve fitting Voltage dependent EL images were captured Eq. (9) used for extracting cell parameters I_{01}, n_1 I_{02}, n_2 parameters estimated by fitting 	<ul style="list-style-type: none"> I_{01}, n_1, I_{02}, n_2 (cell parameters) 	<ul style="list-style-type: none"> First time shown estimation of cell parameters from EL images in non-destructive manner Parameter estimation accuracy in P_{max} with relative error < 3% Useful for cell level quantitative analysis in module manufacturing line Indoor application 	<ul style="list-style-type: none"> Limited applicability to healthy module also not effective for estimating I_{02}, n_2 Requirement of module I-V curve for analysis limits its field applicability 	<ul style="list-style-type: none"> Proposed analytical expression is difficult to extrapolate for commercial size module containing 60/72 cells
	[72,71]	<ul style="list-style-type: none"> Cell-to-cell mismatch LID Finger breakages Mode A and B cracks 	<ul style="list-style-type: none"> Two EL images captured at $0.2I_{sc}$ and I_{sc} 120 modules Terminal current and voltage measurement during EL imaging 	<ul style="list-style-type: none"> Analytical and parametric estimation Two EL images of a test module captured $0.2I_{sc}$ and I_{sc} Using EL images, I_{01} and R_s of individual cell extracted by solving analytical equations Based on extracted I_{01} and n_1, simulation is performed to estimate module P_{out} by generating I-V curve. 	<ul style="list-style-type: none"> I_{01}, R_s (cell) P_{out} (module) 	<ul style="list-style-type: none"> Efficient estimation of module P_{out} with relative error < 3%. Strongly validated on 120 mono c-Si module in indoor and outdoor conditions especially in daylight condition using lock in EL approach considering Si-CCD and InGaAs detector Reproduces I-V curve; hence, study of other performance parameters V_{oc}, FF also possible Outdoor application 	<ul style="list-style-type: none"> Assumption of $n_1 = 1$ makes it suitable for mono c-Si module only. Multi c-Si module n_1 is generally 1.1–1.2. Not applicable if module contain shunting issue as this method assumes $R_{sh} = 1000 \Omega$ Use of spatial analytical equations need high quality and high resolution EL images 	<ul style="list-style-type: none"> This approach evaluates internal cell R_s, in future inclusion of [66] approach of finding external R_s along with this method may increase its applicability to evaluate defects external R_s defects. Requirement of terminal current and voltage measurements and high quality EL images may make outdoor use challenging for each module in large PV field especially with drone-based inspection
	[51]	<ul style="list-style-type: none"> Mode B crack Finger breakages 	<ul style="list-style-type: none"> Two EL images captured at $0.1I_{sc}$ and I_{sc} 3 modules Datasheet information 	<ul style="list-style-type: none"> Analytical expression Two EL images of a test module captured ($>0.3I_{sc}$) and $0.1I_{sc}$ From EL images, cell R_s map estimated by solving analytical equations. Based on R_s map and module datasheet, simulation conducted to estimate module P_{out} 	<ul style="list-style-type: none"> R_s (cell) P_{out} (Module) 	<ul style="list-style-type: none"> Effectively estimate module P_{out} with relative error < 4.3% Outdoor application 	<ul style="list-style-type: none"> Requirement of datasheet information to estimate other cell parameters used in proposed analytical equation Assumption of keeping all other parameters constant makes it only applicable to a new module with R_s defects without any bulk degradation (I_{01}, n_1) 	<ul style="list-style-type: none"> For robustness, it should be tested on different types of modules with different possible R_s defect Estimation of bulk diode parameters using either [71] or [70], instead of datasheet may increase applicability to field-aged modules
	[46]	<ul style="list-style-type: none"> R_s related defects Corrosion 	<ul style="list-style-type: none"> Single EL image captured at I_{sc} 15 modules Module I-V 	<ul style="list-style-type: none"> Machine learning Uses cell-level EL images to classify the cells based on extent of corrosion using EL pixel intensity features in CNN model. Further, calculate the module-level corrosion index based on the cell classes. 	<ul style="list-style-type: none"> R_s (Module) P_{out} (module) 	<ul style="list-style-type: none"> Most efficient power and R_s predicting model has maximum adjusted-R^2 values of 0.88 and 0.73, respectively Use of timely taken EL images enables present and future performance prediction Outdoor application 	<ul style="list-style-type: none"> Proposed ML model requires pre and post-degradation phase module EL images which may be difficult in field condition requiring image processing to eliminate the effect of time varying disturbances 	<ul style="list-style-type: none"> For applying in field condition, timely taken module EL images need to be stored with necessary image correction Future work may be conducted on modifying proposed model to enable estimation of module P_{out} or R_s based on only live EL images without need of past

(continued on next page)

Table 4 (continued)

Literature	Defect and degradation possible to evaluate	Required number of EL images with biasing level, number of PV modules used and other measurements	Approach	Output quantities	Key outcome, Merits and Applicability	Demerits, Limitations and other complexity	Future scope and field application challenges
Shunting defects and degradations	[6]	<ul style="list-style-type: none"> PID-s Process induced shunts, recombination 	<ul style="list-style-type: none"> Two EL images captured at $0.2I_{sc}$ and I_{sc} 2000 modules Terminal measurements for calibration purpose 	<ul style="list-style-type: none"> Predict P_{out} and R_s using polynomial regression model obtained from the module-level corrosion index Empirical method Uses two EL images of attest module captured either before or after degradation or at two EL currents Eq. (10) used to estimate resulted PID-s power loss from the logarithmic ratio of two EL images 	<ul style="list-style-type: none"> P_{loss} (Cell/Module) 	<ul style="list-style-type: none"> Estimate STC P_{loss} with RMSE < 3%. The proposed method have been strongly validated using 2000 EL images Enables prediction of P_{loss} at STC as well as other arbitrary operating conditions of irradiance and temperature Outdoor application 	or pre-degradation stage EL images
	[67]	<ul style="list-style-type: none"> PID-s Process induced shunts, recombination 	<ul style="list-style-type: none"> Two EL images captured at $0.2I_{sc}$ and I_{sc} 10 modules 	<ul style="list-style-type: none"> Empirical method Uses two EL images taken at and $0.2I_{sc}$ and I_{sc} Calculates cell PID-s index taking ratio two EL Eq. (12) enables estimation of cell power loss from PID-s index 	<ul style="list-style-type: none"> P_{loss} (cell) 	<ul style="list-style-type: none"> Estimate cell P_{loss} with relative error < $\pm 3\%$ Applicable to uniform as well as non-uniform PID-s progression considering laboratory to field conditions Simple to use as free from any empirical constant as well as cell or module specific parameter Outdoor application 	<ul style="list-style-type: none"> EL images taken at I_{sc} and $0.9I_{sc}$ may increase ability to quantify severely degraded module at cell and module level Proposed method estimates cell P_{loss} at STC condition only. Generalized correlation predicting loss at other arbitrary operating conditions may be derived like [6]
	[51]	<ul style="list-style-type: none"> Early phase PID-s Weak ohmic shunts 	<ul style="list-style-type: none"> Single EL image captured at $0.07I_{sc}$ 1 module 	<ul style="list-style-type: none"> Analytical approach Use sing low current EL image Eq. (12) enables estimation of module R_s map from single EL image Further, simulation of module based on R_s map estimates module P_{out} 	<ul style="list-style-type: none"> P_{out} (Module) R_{sh} (cell) 	<ul style="list-style-type: none"> Effectively estimate module P_{out} of mild shunted module with relative error < 1% Only single EL image is required for analysis Indoor application 	<ul style="list-style-type: none"> Requirement of at least one healthy cell makes it not applicable for uniformly degraded module Required estimation of calibration factor as well as other cell constants which requires $I-V$ or datasheet information Since this method correlated fall in cell EL intensity with R_{sh}. Results would be erroneous in presence of other defects and degradations
	[69]	<ul style="list-style-type: none"> PID-s Ohmic and non-ohmic shunts Recombination 	<ul style="list-style-type: none"> 4–10 EL images captured at different biases between $0.1I_{sc}$–I_{sc} 10 modules 	<ul style="list-style-type: none"> Analytical and parametric estimation Uses multiple EL images (>4) for quantification. 	<ul style="list-style-type: none"> P_{out} (module) $I_{01}, n_1, I_{02}, n_2, R_s, R_{sh}$ 	<ul style="list-style-type: none"> Estimates cell and module P_{out} with relative error < $\pm 3\%$ Prediction of module output at STC as well as arbitrary 	<ul style="list-style-type: none"> The combine use of EL and IR imaging may be explored for the evaluation of severe form of PID-s Challenging to capture number of EL images at

(continued on next page)

Table 4 (continued)

Literature	Defect and degradation possible to evaluate	Required number of EL images with biasing level, number of PV modules used and other measurements	Approach	Output quantities	Key outcome, Merits and Applicability	Demerits, Limitations and other complexity	Future scope and field application challenges
Multiple defects and degradations	[3]	<ul style="list-style-type: none"> • LID, LeTID • Weak shunting defects • Cell internal R_s defects • Busbar interconnect failures, corrosion 	<ul style="list-style-type: none"> • Terminal measurements for calibration purpose • From EL images, cell parameters are extracted in step-wise manner by solving various equations. • Further, simulations are performed based on extracted parameters to estimate module P_{out} • Analytical approach • Use four EL and DLIT images for quantification • Eq. (8) and Eq. (9) used for the estimation of estimation of cell voltages and R_s from EL images • At the estimated voltages, DLIT used for estimating local I-V of a cell 	<ul style="list-style-type: none"> • P_{out} (Module) • I_{OL}, V_{OC}, FF, P_{out} 	<ul style="list-style-type: none"> operating conditions is possible through simulation • Two stage modeling approach enables cell, submodule and module level quantitative analysis of PID-s degradation • Indoor and outdoor application • Estimate cell P_{out} with relative error < 2%. • Useful in laboratory, for detailed performance analysis of field-aged module by estimation of cell parameters and I-V curve • Indoor application 	<ul style="list-style-type: none"> measurable EL signal for EL current ($\leq I_{sc}$) • Complex to implement and required multiple EL images (>4) depending on the severity of PID-s module 	<ul style="list-style-type: none"> different excitation current in field. • From the view of outdoor application, instead of DLIT, use of passive IR imaging along with EL imaging may be considered for quantification since outdoor passive IR imaging is well established
[22]	[22]	<ul style="list-style-type: none"> • Cell-to-cell mismatches • Weak shunts • Partially disconnected cell 	<ul style="list-style-type: none"> • 10–15 EL images captured at different biases between $0.1I_{sc}$–I_{sc} • 1 module • module dark I-V curve 	<ul style="list-style-type: none"> • P_{out} (cell or module) 	<ul style="list-style-type: none"> • Estimates module P_{out} with relative error < 1–5 % even at low irradiance • Method would be useful where LIT is not available • It would be useful in optimizing cell parameters at the manufacturing end and analyzing degradation in laboratory research • Indoor application 	<ul style="list-style-type: none"> • Use of module dark I-V characteristics limits the applicability of the proposed method to laboratory or indoor use only • Complex to implement 	<ul style="list-style-type: none"> • Need to check applicability to modules with mild to severe from of shunting defects like PID-s
[34,17,15]	[34,17,15]	<ul style="list-style-type: none"> • Weak shunting • Cell internal R_s defects • LID, LeTID • Cell-to-cell mismatches 	<ul style="list-style-type: none"> • 6–15 EL images captured at different biases between $0.1I_{sc}$–I_{sc} • 10–15 modules 	<ul style="list-style-type: none"> • P_{out} (cell or module) 	<ul style="list-style-type: none"> • Estimates P_{out} with relative error < 1% • Non-calibration makes it suitable for field applications • Clearly discussed effect of different EL imaging parameters and gives recommendation for practical applications 	<ul style="list-style-type: none"> • Not applicable to moderate to severely shunted/PID-s modules and I_{ph} related defects • Require high number of EL images • Tedious in building module I-V based in individual cell I-V via parametric extraction 	<ul style="list-style-type: none"> • For outdoor applications, InGaAs camera would be useful for capturing high number of EL images. Also, need of high power fast switching DC power supply for supplying variable current in short duration

(continued on next page)

Table 4 (continued)

Literature	Defect and degradation possible to evaluate	Required number of EL images with biasing level, number of PV modules used and other measurements	Approach	Output quantities	Key outcome, Merits and Applicability	Demerits, Limitations and other complexity	Future scope and field application challenges
[70]	<ul style="list-style-type: none"> Mild to moderate PID-s Busbar interconnect failure Corrosion, back-sheet scratches LID,LeTID Cell-to-cell mismatches 	<ul style="list-style-type: none"> 4–10 EL images captured at different biases between $0.1I_{sc}$–$1.3I_{sc}$ 20 modules Terminal voltage measurements for calibration purpose 	<ul style="list-style-type: none"> Plots I-V curve based on applied EL current and estimated cell voltage to quantify cell/module P_{out} Analytical and parameter extraction Uses 4 to 10 EL images for quantification From EL images, extracts cell/module parameters in step-wise manner solving different equations Based on the extracted parameters performs SDM/DDM simulation to generate module I-V curve and gives module P_{out} 	<ul style="list-style-type: none"> P_{out} (module) 	<ul style="list-style-type: none"> Outdoor application Effectively estimates P_{out} with relative error $<\pm 3\text{--}5\%$ Enables performance evaluation of a module with multiple coexisting defects and degradation Method is generalized, applicable to types of defects and degradations except I_{ph} related and severe PID-s Outdoor application 	<ul style="list-style-type: none"> Does not consider I_{ph} related degradation in quantification. Some steps require manual intervention makes it complex to implement Need number of EL images > 4 	<ul style="list-style-type: none"> In future, an approach for quantifying I_{ph} related degradation may be included in g-QUEL method to expand its applicability For automation and to increase field applicability, ML may be used in some steps to reduce need of manual intervention

- In quantifying optical defects and degradations, machine learning or empirical approaches may be preferred over the parametric extraction approach in the future development of quantitative EL methods.

5.2. Bulk diode and series resistance related issues

Table 4 shows that the parametric estimation approach has been mostly used for evaluating bulk diode and R_s related issues. Bauer et al. and Rajput et al. [3,71] method enables quantifying sub-cell as well as cell level impact of bulk defects using two EL images. The EL sweep and g-QUEL methods (Section 3.2.4.3 and 3.2.4.4) also effectively evaluate bulk defects using multiple EL images. Cell R_s -related defects are primarily divided into two categories: internal (finger breakages, mode B cracks) and external (interconnect failure, metallic corrosion, increased contact resistance) [66]. The method proposed by [51] and [71] quantify cell internal R_s only as these methods estimate spatial distribution of R_s within a cell with respect to brightest point closer to busbar in an EL image (Eq. (7)). R_s related defects external to cell such as increased contact resistance between cell-to-cell interconnects may not reflect a specific pattern or signature in an EL images. Use of Eq. (9), only enables estimation of cumulative cell R_s , as in this equation difference between measured module terminal voltage and summation of estimated cell voltages is divided by product of EL current and total number of cells. Hence, estimated R_s using Eq. (9) contains cumulative impact of all R_s components. The methods reported by [66,46,70] allow evaluating cumulative module level impact of all R_s defects.

- Overall, the proposed quantitative EL methods are well reported for evaluating impact of bulk diode, and series resistance related problems and show good accuracy in quantification.
- For estimation of cell or module R_s , at least two EL images and terminal voltage measurement requires for most of the methods, which may be difficult in a field.

5.3. Shunting defects and degradations

Empirical methods [6,67] are simple for estimating PID-s power loss using the ratio of two EL images. General empirical correlation of [67] is free from any constant and is easy to use in outdoor condition on the cost of accuracy. QELA method is capable of estimating PID-s loss at STC as well as other operating conditions. Novel QUEL method provides a thorough analysis of PID-s at the cell and module levels with high accuracy. However, the requirement of multiple EL images and module calibration makes it complex as compared with empirical methods.

In PID-s assessment, EL current (biasing level) plays an essential role in evaluating module performance. For checking PID-s susceptibility, low biasing level ($0.1I_{sc}$) have been suggested in IEC TS 62804–1 and

IEC TS 60904–13. While considering the quantitative analysis, it is necessary that cell should have finite active EL emission for processing signal. As PID-s severity increases, images captured at a low biasing level show a completely dark appearance due to lack of EL emission; consequently, no quantitative information can be extracted. Considering practical application, this review suggests using biasing level $I_{EL} \geq 0.2I_{sc}$ for dealing with the initial to moderate phase of PID-s. For severe form of PID-s, a higher biasing level about I_{sc} should be used to extract optimal quantitative information from EL images. For a non-shunted module, it is relatively straightforward to apply a set of EL currents and measure individual cell voltages to generate cell I - V curve, as shown by [15] and [66]. However, as mentioned in Section 2.1, shunted cells do not emit EL emissions at low biasing levels (see Fig. 5(d)), which makes the quantification of shunting defects and degradation a challenging task, as illustrated in Fig. 24 [34,62].

Puranik and Gupta [69] have overcome this limitation by using the current-EL intensity curve instead of the voltage-EL intensity for estimating mild to moderate forms of PID-s. However, this approach also cannot quantify severe forms of PID-s as cell does not emit measurable EL signal for the applied range of EL excitation current ($\leq I_{sc}$). In severely degraded cells, shunt defect sinks the significant fraction of EL current, and negligible current flows through the p - n junction diode which is responsible for EL emission. Hence, beyond certain limit EL imaging can not evaluate severe form of PID-s. In that case, IR imaging [44] can be used as it maps shunted cell based on temperature profile. For effective evaluation a module with cell having different extent of PID-s, use of IR imaging along with EL may give better performance of quantification. Also, low current EL image saturates early; hence, use of low current EL images limits the range of quantification e.g., [51,67]. Use of possibly high current EL images may extend the possible range of quantification.

- The existing methods show good performance in quantifying the impact of shunting defects and degradations.
- The quantification of severe forms of PID-s using EL imaging remains a challenge for the future.
- To overcome the limitations of EL imaging in quantifying PID-s, the combination of IR imaging with EL imaging may be considered in the future, as mild to severe forms of shunting can be distinguished from IR images.

5.4. Multiple defects and degradations

Combining I - V , DLIT or QE techniques with EL allows a comprehensive analysis of PV modules. Although, these methods require extensive measurements and are only suitable for indoor degradation analysis. EL sweep and g-QUEL methods are generalized and capable of assessing multi-defect and degradation except severe shunting and

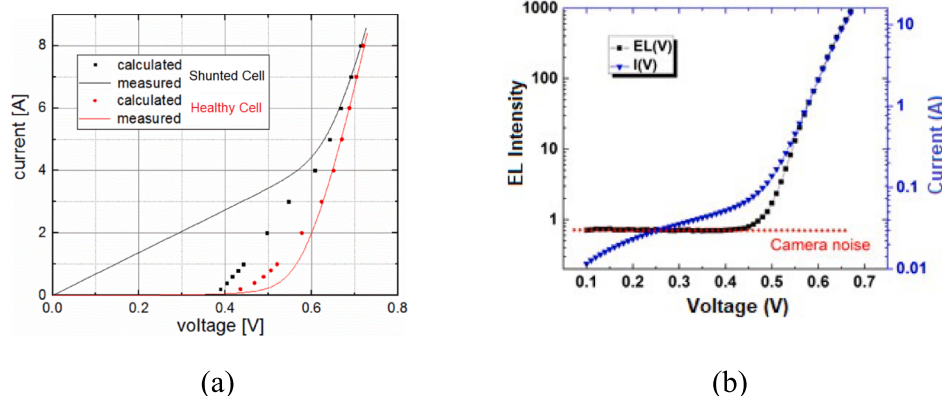


Fig. 24. (a) Comparison of experimental and simulated cell I - V curve (reproduced from [34]) (b) Comparison of cell curve obtained from I to V and EL measurements (reproduced from [62]).

optical defects. EL sweep method does not require calibration, which increases its field applicability. However, it is not applicable to mild to moderate shunting defects and involves more calculations for module level use. The g-QUEL method can assess mild to severe forms of shunting. Compared with EL sweep, the g-QUEL method directly estimates cell/module parameters from the stack of EL images on the cost of module calibration. Both methods employ a parametric extraction approach to determine module P_{out} accurately.

- Future work may focus on making these methods more simplified and automated and reducing the required input EL images.
- To increase generalization, the ability to quantify optical and severe shunting defects needs to be included. A machine learning approach could be useful to quantify optical defects, while IR imaging may be effective in identifying severe shunting, as discussed in Section 3.1.3 and 3.3.5, respectively.

6. Conclusions

This article thoroughly reviewed the progress of module-level quantitative EL imaging. The reported literature for a different category of defect and degradation has been evaluated based on the approach of quantification, input EL imaging requirement, and performance of quantification. Comparative analysis of the quantitative EL methods for each category of defects and degradation has also been presented. The key outcome of this review has been summarized below.

Quantification of various defects and degradations

- Quantitative EL methods for bulk and series resistance degradation are well-reported. These defects are relatively easy to quantify compared with other categories of defects.
- Most existing methods effectively quantify mild to moderate shunting defects, especially PID-s. Severely shunted module emits a very weak EL signal; hence, EL imaging cannot quantify severe shunting defects and degradations beyond a certain point. In the future, to address this problem, quantitative EL methods can consider the possible use of IR or DLIT imaging along with EL for quantifying severe forms of PID-s. IR image maps cell temperatures and can clearly distinguish mild to severe forms of PID-s. Combination of EL and IR can enable detailed performance analysis of severely affected PID-s modules. For detailed cell/sub-cell level quantitative analysis, DLIT may also be explored to estimate localized power loss caused by severe PID-s defects within a cell along with EL imaging.
- Existing literature on quantification of optical defects and degradation is inadequate. So far, quantitative EL imaging for cell breakages and soft soiling has been discussed in the literature which still has scope further to improve the accuracy of quantification. Future research can be dedicated to the development of methods to evaluate impact of major optical defects such discoloration, delamination or hard soiling, which are predominantly observed in a field.
- Majority of quantitative EL methods evaluate particular type of defects and degradation. While a few generalized methods like EL sweep and g-QUEL method can evaluate the performance of a module with multiple defects and degradations. However, challenges exist considering the possible inclusion of optical and severe shunting defects and need to be addressed in future.

Quantification approaches

- Parametric extraction is the most preferred approach among the reported quantitative EL method. The method following this approach extracts more quantitative information, including cell or module parameters along with module output power. Methods proposed by [13,51,69,71] have been developed for a particular type of defect to extract one or few cell parameters. Whereas methods EL

Sweep and g-QUEL extract most of cell parameters enabling performance analysis of module with different types of defects. Compared to other approaches, parametric extraction approach enables detailed quantitative analysis at STC or other arbitrary set of operating conditions. However, it requires greater number of EL images and is complex to implement.

- Empirical approach [6,23,67] is easy to implement and mostly based on a single empirical correlation in which relative fall or change in EL intensity is correlated with resulted power loss. Hence, it enables estimating cell/module power loss caused by particular defect based on two EL images captured either before or after defect progression or two different EL current (using low and high biasing levels). Compared to parametric extraction methods, empirical approach does not provide detailed quantitative information.
- ML approaches [46,74] are also easy to use and quantifies module performance primarily based on processing of a single EL image. However, the development of ML method is complex and requires a very high number of EL images for training algorithm. Similar to empirical approach, ML approach also provides limited quantitative information.
- Use of EL imaging with I-V [22], DLIT [3], QE [13] combines the advantages of individual techniques and enables detailed quantitative analysis of a module with different types of defects and degradations. EL imaging has good capabilities of mapping cell/sub-cell level voltage, whereas DLIT or QE offers sub-cell level current measurements. Combining EL with other techniques offers detailed qualitative and quantitative information on the cost of increased experimental requirements which limits its outdoor applicability.

Quantification performance and applicability

- Most of the reported quantitative EL method shows good accuracy in evaluating module power with relative error $\leq \pm 3\text{--}5\%$.
- For detailed quantitative analysis of bulk, series resistance, and shun-related defects, parametric extraction is more suitable as it enables simulating module output at different levels. However, the requirement of capturing multiple EL images and auxiliary measurements may limit its outdoor applicability to string level or small PV plant.
- For the sole estimation of power losses resulting from cell breakages, or PID-s, empirical and ML approaches are more suitable. Since the requirement of these approaches is mostly single or two EL images; hence, outdoor application for large number of modules is possible.
- Use of multi-characterization approaches enables detailed quantitative analysis of a defective PV module; however, it has limited applicability of indoor conditions only.
- Future research may be focused on achieving good accuracy while applying the reported quantitative EL methods in outdoor conditions. Also, work may be dedicated to expand their capability to quantify defects and degradation such as severe forms of PID-s, discoloration, delamination, hard soiling that have not been fully quantitatively characterized yet by EL imaging.

This review will be useful for the future growth of quantitative EL imaging, considering the development of new quantitative EL methods and their possible application in a PV field.

Declaration of Competing Interest

The authors declare that they have no known competing financial interests or personal relationships that could have appeared to influence the work reported in this paper.

References

- [1] Aghaei, M., Fairbrother, A., Gok, A., Ahmad, S., Kazim, S., Lobato, K., Oreski, G., Reinders, A., Schmitz, J., Theelen, M., Yilmaz, P., Kettle, J., 2022. Review of

- degradation and failure phenomena in photovoltaic modules. *Renew. Sustain. Energy Rev.* 159, 112160. <https://doi.org/10.1016/j.rser.2022.112160>.
- [2] Bartler, A., Mauch, L., Yang, B., Reuter, M., Stoicescu, L., 2018. Automated detection of solar cell defects with deep learning, in: 26th European Signal Processing Conference (EUSIPCO). EURASIP, pp. 2035–2039. 10.23919/EUSIPCO.2018.8553025.
- [3] Bauer, J., Fröhlauf, F., Breitenstein, O., 2017. Quantitative local current-voltage analysis and calculation of performance parameters of single solar cells in modules. *Solar Energy Mater. Solar Cells* 159, 8–19. <https://doi.org/10.1016/j.solmat.2016.08.029>.
- [4] Bedrich, K., 2017. Quantitative electroluminescence measurements of PV devices. Loughborough University.
- [5] Bedrich, K., Bokalic, M., Bliss, M., Topic, M., Betts, T.R., Gottschalg, R., 2018. Electroluminescence Imaging of PV Devices: Advanced Vignetting Calibration. *IEEE J. Photovoltaics* 8, 1297–1304. <https://doi.org/10.1109/JPHOTOV.2018.2848722>.
- [6] Bedrich, K.G., Luo, W., Pravettoni, M., Chen, D., Chen, Y., Wang, Z., Verlinden, P.J., Hacke, P., Feng, Z., Chai, J., Wang, Y., Aberle, A.G., Khoo, Y.S., 2018. Quantitative Electroluminescence Imaging Analysis for Performance Estimation of PID-Influenced PV Modules. *IEEE J. Photovoltaics* 8 (5), 1281–1288.
- [7] Bordihn, S., Fladung, A., Schlipf, J., Kontges, M., Köntges, M., 2022. Machine Learning Based Identification and Classification of Field-Operation Caused Solar Panel Failures Observed in Electroluminescence Images. *IEEE J. Photovoltaics* 12, 827–832. <https://doi.org/10.1109/JPHOTOV.2022.3150725>.
- [8] Breitenstein, O., 2012. Local efficiency analysis of solar cells based on lock-in thermography. *Sol. Energy Mater. Sol. Cells* 107, 381–389. <https://doi.org/10.1016/j.solmat.2012.07.019>.
- [9] Breitenstein, O., 2011. Nondestructive local analysis of currentvoltage characteristics of solar cells by lock-in thermography. *Sol. Energy Mater. Sol. Cells* 95, 2933–2936. <https://doi.org/10.1016/j.solmat.2011.05.049>.
- [10] Breitenstein, O., Bauer, J., Bothe, K., Hinken, D., Muller, J., Kwapił, W., Schubert, M.C., Warta, W., 2011. Can luminescence imaging replace lock-in thermography on solar cells and wafers? *IEEE J. Photovoltaics* 1, 000062. <https://doi.org/10.1109/jpsc.2011.6185846>.
- [11] Breitenstein, O., Khanna, A., Augarten, Y., Bauer, J., Wagner, J.M., Iwig, K., 2010. Quantitative evaluation of electroluminescence images of solar cells. *Phys. Status Solidi - Rapid Res. Lett.* 4, 7–9. <https://doi.org/10.1002/pssr.200903304>.
- [12] Breitenstein, O., Rakotonainaina, J.P., Al Rifai, M.H., Werner, M., 2004. Shunt types in crystalline silicon solar cells. *Prog. Photovolt. Res. Appl.* 12, 529–538. <https://doi.org/10.1002/PIP.544>.
- [13] Castañeda, C.A.R., Chattopadhyay, S., Oh, J., Tatapudi, S., Mani, G.T., Hu, H., Rodríguez Castañeda, C.A., Chattopadhyay, S., Oh, J., Tatapudi, S., Mani, G.T., Hu, H., 2017. Field inspection of PV modules: Quantitative determination of performance loss due to cell cracks using EL images. *Data Compression Conf. Proc.* 2017-March, 1858–1862. 10.1109/PVSC.2017.8366560.
- [14] Chen, D., Vaqueiro, M., Ciesla, A., Phillip, H., Hallam, B., Abbott, M., Chan, C., 2021. Progress in the understanding of light- and elevated temperature-induced degradation in silicon solar cells: A review. *Prog. Photovolt. Res. Appl.* 29, 1180–1201. <https://doi.org/10.1002/PIP.3362>.
- [15] Colvin, D.J., Schneller, E.J., Davis, K.O., 2022. Cell dark current-voltage from non-calibrated module electroluminescence image analysis. *Sol. Energy* 244, 448–456. <https://doi.org/10.1016/j.solener.2022.08.043>.
- [16] Colvin, D.J., Schneller, E.J., Davis, K.O., 2021. Impact of interconnection failure on photovoltaic module performance. *Prog. Photovolt. Res. Appl.* 29, 524–532. <https://doi.org/10.1002/PIP.3401>.
- [17] Colvin, D.J., Schneller, E.J., Davis, K.O., 2019. Extracting Cell Level Characteristics from Photovoltaic Module Electroluminescence Images. *Conf. Rec. IEEE Photovolt. Spec. Conf.* 2740–2742 <https://doi.org/10.1109/PVSC40753.2019.8981212>.
- [18] Colvin, D.J., Schneller, E.J., Horner, G.S., Gabor, A.M., Davis, K.O., 2021. Evaluating Impact on Electroluminescence Image Quality and Quantitative Analysis using Different Camera Technologies. *Conf. Rec. IEEE Photovolt. Spec. Conf.* 1057–1061 <https://doi.org/10.1109/PVSC43889.2021.9518826>.
- [19] Deceglie, M.G., Silverman, T.J., Johnston, S.W., Rand, J.A., Reed, M.J., Flottemesch, R., Repins, I.L., 2020. Light and Elevated Temperature Induced Degradation (LeTID) in a Utility-Scale Photovoltaic System. *IEEE J. Photovoltaics* 10, 1084–1092. <https://doi.org/10.1109/JPHOTOV.2020.2989168>.
- [20] Deitsch, S., Christlein, V., Berger, S., Buerhop-Lutz, C., Maier, A., Gallwitz, F., Riess, C., 2019. Automatic classification of defective photovoltaic module cells in electroluminescence images. *Sol. Energy* 185, 455–468. <https://doi.org/10.1016/j.solener.2019.02.067>.
- [21] Demirci, M.Y., Beşli, N., Güümüşü, A., 2021. Efficient deep feature extraction and classification for identifying defective photovoltaic module cells in Electroluminescence images. *Expert Syst. Appl.* 175, 114810.
- [22] Dix-Peek, R.M., van Dyk, E.E., Vorster, F.J., 2021. Maximum power estimation through injection dependent electroluminescence imaging. *Energy Sci. Eng.* 9, 757–767. <https://doi.org/10.1002/ese.3.858>.
- [23] Doll, B., Forberich, K., Hepp, J., Langner, S., Buerhop-Lutz, C., Hauch, J.A., Brabec, C.J., Peters, I.M., 2022. Luminescence Analysis of PV-Module Soiling in Germany. *IEEE J. Photovoltaics* 12, 81–87. <https://doi.org/10.1109/JPHOTOV.2021.3123076>.
- [24] Doll, B., Hepp, J., Hoffmann, M., Schuler, R., Buerhop-Lutz, C., Peters, I.M., Hauch, J.A., Maier, A., Brabec, C.J., 2021. Photoluminescence for Defect Detection on Full-Sized Photovoltaic Modules. *IEEE J. Photovoltaics* 11, 1419–1429. <https://doi.org/10.1109/JPHOTOV.2021.3099739>.
- [25] Dost, G., Höffler, H., Greulich, J.M., 2021. Advanced Series Resistance Imaging for Silicon Solar Cells via Electroluminescence. *Phys. Status Solidi Appl. Mater. Sci.* 218 <https://doi.org/10.1002/pssa.202000546>.
- [26] Fahrland, C., Ludwig, Y., Kersten, F., Petter, K., 2014. Sponge LID - A new degradation mechanism?, in: 40th IEEE Photovoltaic Specialist Conference, pp. 135–139. <https://doi.org/10.1109/PVSC.2014.6925400>.
- [27] Fiorese, J., Colvin, D.J., Frota, R., Gupta, R., Li, M., Seigneur, H.P., Vyas, S., Oliveira, S., Shah, M., Davis, K.O., 2022. Automated Defect Detection and Localization in Photovoltaic Cells Using Semantic Segmentation of Electroluminescence Images. *IEEE J. Photovoltaics* 12, 53–61. <https://doi.org/10.1109/JPHOTOV.2021.3131059>.
- [28] Fraunhofer, 2022. Photovoltaics Report 27/07/2022. Fraunhofer ISE - PSE.
- [29] Fruehauf, F., Turek, M., 2015. Quantification of Electroluminescence Measurements on Modules. *Energy Procedia* 77, 63–68. <https://doi.org/10.1016/j.egypro.2015.07.010>.
- [30] Fuyuki, T., Kitayanan, A., 2009. Photographic diagnosis of crystalline silicon solar cells utilizing electroluminescence. *Appl. Phys. A Mater. Sci. Process.* 96, 189–196. <https://doi.org/10.1007/s00339-008-4986-0>.
- [31] Fuyuki, T., Kondo, H., Kaji, Y., Ogane, A., Takahashi, Y., 2007. Analytic findings in the electroluminescence characterization of crystalline silicon solar cells. *J. Appl. Phys.* 101, 1–5. <https://doi.org/10.1063/1.2431075>.
- [32] Fuyuki, T., Kondo, H., Yamazaki, T., Takahashi, Y., Uraoka, Y., 2005. Photographic surveying of minority carrier diffusion length in polycrystalline silicon solar cells by electroluminescence. *Appl. Phys. Lett.* 86, 1–3. <https://doi.org/10.1063/1.1978979>.
- [33] Glatthaar, M., Haunschmid, J., Zeidler, R., Demant, M., Greulich, J., Michl, B., Warta, W., Rein, S., Preu, R., 2010. Evaluating luminescence based voltage images of silicon solar cells. *J. Appl. Phys.* 108, 1–6. <https://doi.org/10.1063/1.3443438>.
- [34] Guo, S., Schneller, E., Davis, K.O., Schoenfeld, W.V., 2016. Quantitative analysis of crystalline silicon wafer PV modules by electroluminescence imaging. In: IEEE 43rd Photovoltaic Specialists Conference (PVSC). IEEE, pp. 3688–3692. <https://doi.org/10.1109/PVSC.2016.7750365>.
- [35] Hinken, D., Ramspeck, K., Bothe, K., Fischer, B., Brendel, R., 2007. Series resistance imaging of solar cells by voltage dependent electroluminescence. *Appl. Phys. Lett.* 91, 89–92. <https://doi.org/10.1063/1.2804562>.
- [36] Hoffmann, M., Buerhop-Lutz, C., Reeb, L., Pickel, T., Winkler, T., Doll, B., Würfl, T., Marius Peters, I., Brabec, C., Maier, A., Christlein, V., 2021. Deep-learning-based pipeline for module power prediction from electroluminescence measurements. *Prog. Photovolt. Res. Appl.* 29, 920–935. <https://doi.org/10.1002/PIP.3416>.
- [37] Hoiaas, I., Grujic, K., Imenes, A.G., Burud, I., Olsen, E., Belbachir, N., 2022. Inspection and condition monitoring of large-scale photovoltaic power plants: A review of imaging technologies. *Renew. Sustain. Energy Rev.* 161, 112353. <https://doi.org/10.1016/j.rser.2022.112353>.
- [38] IEC, 2018. Photovoltaic devices - Part 13: Electroluminescence of photovoltaic modules, IEC 60904-13.
- [39] IEC standard 62804-1, 2020.
- [40] Ishaque, K., Salam, Z., Taheri, H., 2011. Simple, fast and accurate two-diode model for photovoltaic modules. *Sol. Energy Mater. Sol. Cells* 95, 586–594. <https://doi.org/10.1016/j.solmat.2010.09.023>.
- [41] Ishikawa, Y., 2022. Outdoor evaluation of photovoltaic modules using electroluminescence method. *JSAP Rev.* 1–5.
- [42] Jahn, U., Herz, M., Rheinland, T., 2018. Review on Infrared (IR) and Electroluminescence (EL) imaging for photovoltaic field applications, IEA-Photovoltaic Power Systems Programme.
- [43] Jordan, D.C., Silverman, T.J., Wohlgemuth, J.H., Kurtz, S.R., VanSant, K.T., 2015. Photovoltaic failure and degradation modes. *Prog. Photovolt. Res. Appl.* 20, 6–11. <https://doi.org/10.1002/PIP>.
- [44] Kaden, T., Lammers, K., Möller, H.J., 2015. Power loss prognosis from thermographic images of PID affected silicon solar modules. *Sol. Energy Mater. Sol. Cells* 142, 24–28. <https://doi.org/10.1016/j.solmat.2015.05.028>.
- [45] Karimi, A.M., Fada, J.S., Hossain, M.A., Yang, S., Peshek, T.J., Braid, J.L., French, R.H., 2019. Automated Pipeline for Photovoltaic Module Electroluminescence Image Processing and Degradation Feature Classification. *IEEE J. Photovoltaics* 9, 1324–1335. <https://doi.org/10.1109/JPHOTOV.2019.2920732>.
- [46] Karimi, A.M., Fada, J.S., Parrilla, N.A., Pierce, B.G., Koyuturk, M., French, R.H., Braid, J.L., 2020. Generalized and Mechanistic PV Module Performance Prediction from Computer Vision and Machine Learning on Electroluminescence Images. *IEEE J. Photovoltaics* 10, 878–887. <https://doi.org/10.1109/JPHOTOV.2020.2973448>.
- [47] Kersten, F., Fertig, F., Petter, K., Klöter, B., Herzog, E., Strobel, M.B., Heitmann, J., Müller, J.W., 2017. System performance loss due to LeTID. *Energy Procedia* 124, 540–546. <https://doi.org/10.1016/j.egypro.2017.09.260>.
- [48] Kikelj, M., Lipov, B., Lipovšek, B., Bokalić, M., Topić, M., 2021. Spatially resolved electrical modelling of cracks and other inhomogeneities in crystalline silicon solar cells. *Prog. Photovolt. Res. Appl.* 29, 124–133. <https://doi.org/10.1002/PIP.3348>.
- [49] Kim, J., Rabelo, M., Padi, S.P., Younsif, H., Cho, E.C., Yi, J., 2021. A review of the degradation of photovoltaic modules for life expectancy. *Energies* 14. <https://doi.org/10.3390/en14144278>.
- [50] Koester, L., Lindig, S., Louwen, A., Astigarraga, A., Manzolini, G., Moser, D., 2022. Review of photovoltaic module degradation, field inspection techniques and techno-economic assessment. *Renew. Sustain. Energy Rev.* 165, 112616. <https://doi.org/10.1016/j.rser.2022.112616>.
- [51] Kropp, T., Schubert, M., Werner, J., 2018. Quantitative prediction of power loss for damaged photovoltaic modules using electroluminescence. *Energies* 11 (5), 1172.

- [52] Kumar, S., Meena, R., Gupta, R., 2021. Finger and interconnect degradations in crystalline silicon photovoltaic modules: A review. *Sol. Energy Mater. Sol. Cells* 230, 111296. <https://doi.org/10.1016/j.solmat.2021.111296>.
- [53] Kumar, S., Meena, R., Mohammed, H., Gupta, R., 2020. Degradation in crystalline silicon photovoltaic modules under hot climate conditions. in: international Conference on Vision of Solar Energy in the Kingdom of Saudi Arabia: Applications and Challenges (VSESA2020). Saudi Arabia.
- [54] Kunz, O., Schlipf, J., Fladung, A., Khoo, Y.S., Bedrich, K., Trupke, T., Hameiri, Z., 2022. Outdoor luminescence imaging of field-deployed PV modules. *Prog. Energy* 4 (4), 042014.
- [55] Lindroos, J., Savin, H., 2016. Review of light-induced degradation in crystalline silicon solar cells. *Sol. Energy Mater. Sol. Cells* 147, 115–126. <https://doi.org/10.1016/j.solmat.2015.11.047>.
- [56] Luo, W., Khoo, Y.S., Hacke, P., Naumann, V., Lausch, D., Harvey, S.P., Singh, J.P., Chai, J., Wang, Y., Aberle, A.G., Ramakrishna, S., 2017. Potential-induced degradation in photovoltaic modules: A critical review. *Energ. Environ. Sci.* 10, 43–68. <https://doi.org/10.1039/c6ee02271e>.
- [57] Manganiello, P., Balato, M., Vitelli, M., 2015. A Survey on Mismatching and Aging of PV Modules: The Closed Loop. *IEEE Trans. Ind. Electron.* 62, 7276–7286. <https://doi.org/10.1109/TIE.2015.2418731>.
- [58] Mantel, C., Villebro, F., Alves, G., Parikh, H.R., Wendlandt, S., Mantel, C., Villebro, F., Alves, G., Rajesh, H., Wendlandt, S., Hossain, K., Poulsen, P.B., Spataru, S., Alves dos Reis Benatto, G., Rajesh Parikh, H., Wendlandt, S., Hossain, K., Poulsen, P.B., Spataru, S., Séra, D., Forchhammer, S., 2019. Machine learning prediction of defect types for electroluminescence images of photovoltaic panels, in: SPIE Conference Proceedings. p. 1. 10.1117/12.2528440.
- [59] Meena, R., Niyaz, H.M., Gupta, R., 2023. Investigation and Differentiation of Degradation Modes Affecting Series Resistance in Photovoltaic Cells and Modules. *IEEE J. Photovoltaics* 13, 283–290. <https://doi.org/10.1109/JPHOTOV.2023.3239744>.
- [60] Mehta, H.K., Warke, H., Kukadiya, K., Panchal, A.K., 2019. Accurate Expressions for Single-Diode-Model Solar Cell Parameterization. *IEEE J. Photovoltaics* 9, 803–810. <https://doi.org/10.1109/JPHOTOV.2019.2896264>.
- [61] Mochizuki, T., Kim, C., Yoshita, M., Mitchell, J., Lin, Z., Chen, S., Takato, H., Kanemitsu, Y., Akiyama, H., 2016. Solar-cell radiance standard for absolute electroluminescence measurements and open-circuit voltage mapping of silicon solar modules. *J. Appl. Phys.* 119 <https://doi.org/10.1063/1.4940159>.
- [62] Ory, D., Paul, N., Lombez, L., 2021. Extended quantitative characterization of solar cell from calibrated voltage-dependent electroluminescence imaging. *J. Appl. Phys.* 129 <https://doi.org/10.1063/5.0021095>.
- [63] Parikh, H.R., Buratti, Y., Spataru, S., Villebro, F., Reis Benatto, G.A.D., Poulsen, P.B., Wendlandt, S., Kerekes, T., Séra, D., Hameiri, Z., 2020. Solar cell cracks and finger failure detection using statistical parameters of electroluminescence images and machine learning. *Appl. Sci.* 10 (24), 8834.
- [64] Petrone, G., Andres, C., Ramos, G., Spagnuolo, C.A., Ramos-Paja, G., 2017. Spagnuolo Photovoltaic Sources Modeling. *Photovoltaic Sources Modeling. John Wiley & Sons*, 10.1002/9781118755877.
- [65] Pingel, S., Frank, O., Winkler, M., Oaryan, S., Geipel, T., Hoehne, H., Berghold, J., 2010. Potential induced degradation of solar cells and panels, in: 35th IEEE Photovoltaic Specialists Conference. pp. 2817–2822. 10.1109/PVSC.2010.5616823.
- [66] Potthoff, T., Bothe, K., Eitner, U., Hinken, D., König, M., 2010. Detection of the voltage distribution in photovoltaic modules by electroluminescence imaging. *Prog. Photovolt. Res. Appl.* 18, 100–106. <https://doi.org/10.1002/pip.941>.
- [67] Puranik, V.E., Gupta, R., 2022. Standardized applications of electroluminescence imaging for efficient investigation of potential-induced degradation shunting in crystalline silicon photovoltaic module. *Sol. Energy* 245, 183–192. <https://doi.org/10.1016/j.solener.2022.09.014>.
- [68] Puranik, V.E., Gupta, R., 2022. Analysis and insight of electroluminescence imaging in the assessment of potential-induced degradation in crystalline silicon photovoltaic module. *Eng. Fail. Anal.* 134, 106027 <https://doi.org/10.1016/j.engfailanal.2022.106027>.
- [69] Puranik, V.E., Gupta, R., 2021. Novel Quantitative Electroluminescence Method for Detailed Performance Analysis of PID-s Affected Crystalline Silicon PV Module. *IEEE J. Photovoltaics* 11, 1470–1478. <https://doi.org/10.1109/JPHOTOV.2021.3108764>.
- [70] Puranik, V.E., Kumar, R., Gupta, R., 2023. Generalized quantitative electroluminescence method for the performance evaluation of defective and unevenly degraded crystalline silicon photovoltaic module. *Prog. Photovolt. Res. Appl.* 31, 269–282. <https://doi.org/10.1002/pip.3632>.
- [71] Rajput, A.S., Ho, J.W., Zhang, Y., Nalluri, S., Aberle, A.G., 2018. Quantitative estimation of electrical performance parameters of individual solar cells in silicon photovoltaic modules using electroluminescence imaging. *Sol. Energy* 173, 201–208. <https://doi.org/10.1016/j.solener.2018.07.046>.
- [72] Rajput, A.S., Zhang, Y., Rodriguez-Gallegos, C.D., Khanna, A., Basu, P.K., Nalluri, S., Singh, J.P., 2020. Comparative Study of the Electrical Parameters of Individual Solar Cells in a c-Si Module Extracted Using Indoor and Outdoor Electroluminescence Imaging. *IEEE J. Photovoltaics* 10, 1396–1402. <https://doi.org/10.1109/JPHOTOV.2020.3001720>.
- [73] Rau, U., 2007. Reciprocity relation between photovoltaic quantum efficiency and electroluminescent emission of solar cells. *Phys. Rev. B - Condens. Matter Mater. Phys.* 76, 1–8. <https://doi.org/10.1103/PhysRevB.76.085303>.
- [74] Rodrigues, S., Buerhop, C., Doll, B., Hauch, J., Brabec, C., Peters, M., 2020. Predicting Module IV curve from EL images using machine learning, in: 37th European Photovoltaic Solar Energy Conference and Exhibition, EU-PVSEC. pp. 1364–1369.
- [75] Roy, S., Gupta, R., 2019. Quantitative Estimation of Shunt Resistance in Crystalline Silicon Photovoltaic Modules by Electroluminescence Imaging. *IEEE J. Photovoltaics* 9, 1741–1747. <https://doi.org/10.1109/JPHOTOV.2019.2930402>.
- [76] Serfa Juan, R.O., Kim, J., 2020. Photovoltaic Cell Defect Detection Model based-on Extracted Electroluminescence Images using SVM Classifier, in: International Conference on Artificial Intelligence in Information and Communication (ICAIC). IEEE, pp. 578–582. 10.1109/ICAIC48513.2020.9065065.
- [77] Shioda, T., 2013. Delamination failures in long-term field-aged PV modules from point of view of encapsulant, 2013 NREL PV Module Reliability Workshop. 10.21832/9781845414122-016.
- [78] Simon, K., Thomas, W., Christian, S., Andreas, F., Patrick, C., Juliane, B., 2007. Electroluminescence Imaging of Crystalline Photovoltaic Modules: Comparative Study Between Manual Ground-Level Inspections and Drone-Based Aerial Surveys. 32nd Eur. Photovolt. Sol. Energy Conf. Exhib. 5, 6–38.
- [79] Sinha, A., Sastry, O.S., Gupta, R., 2016. Nondestructive characterization of encapsulant discoloration effects in crystalline-silicon PV modules. *Sol. Energy Mater. Sol. Cells* 155, 234–242. <https://doi.org/10.1016/j.solmat.2016.06.019>.
- [80] Sopori, B., Basnyat, P., Devayajanan, S., Shet, S., Mehta, V., Binns, J., Appel, J., 2012. Understanding Light-Induced Degradation of c-Si Solar Cells, in: 38th IEEE Photovoltaic Specialists Conference. IEEE, pp. 1115–1120. 10.1109/PVSC.2012.6317798.
- [81] Spataru, S., Hacke, P., Sera, D., Glick, S., Kerekes, T., Teodorescu, R., 2015. Quantifying solar cell cracks in photovoltaic modules by electroluminescence imaging. 2015 IEEE 42nd Photovolt. Spec. Conf. PVSC 2015, 1–6. <https://doi.org/10.1109/PVSC.2015.7356124>.
- [82] Tang, W., Yang, Q., Xiong, K., Yan, W., 2020. Deep learning based automatic defect identification of photovoltaic module using electroluminescence images. *Sol. Energy* 201, 453–460. <https://doi.org/10.1016/j.solener.2020.03.049>.
- [84] Trupke, T., 2007. Spatially resolved series resistance of silicon solar cells obtained from luminescence.pdf. *Appl. Phys. Lett.* 90 <https://doi.org/10.1063/1.2709630>.
- [85] Wang, H., Cheng, X., Yang, H., He, W., Chen, Z., Xu, L., Song, D., 2019. Potential-induced degradation: Recombination behavior, temperature coefficients and mismatch losses in crystalline silicon photovoltaic power plant. *Sol. Energy* 188, 258–264. <https://doi.org/10.1016/j.solener.2019.06.023>.